Quantitative characterisation of the influence of different environmental factors on coal spontaneous combustion

Jingyu Zhao[1,2] · Chen Wang[1] · Jiajia Song[1] · Shiping Lu[1] · Jun Deng[2] · Yanni Zhang[1] · Chi-Min Shu[3]

Abstract

Coal spontaneous combustion (CSC) events pose hazards to miners, infrastructure, and the environment. To mitigate some of the risk of CSC, this study explored the influence of airflow rate (AFR), oxygen concentration (OxyC), and heating rate (HR) on CSC. A temperature programmed experiment was used to examine a coal sample under different AFRs, OxyCs, and HRs. The characteristic temperature was determined using index gas growth rate analysis, and the characteristic parameters were shown. The apparent activation energy (E_a) of the sample was computed by the Arrhenius equation, and variance analysis was employed to quantitatively characterise the impact of different environmental factors on the characteristic parameters of the coal samples. The experimental results show that the critical temperature of the coal samples ranges between 65 and 75 °C, and the cracking temperature ranges between 115 and 130 °C, dividing the low-temperature oxidation process of coal into three stages: before the critical temperature, between the critical temperature and the cracking temperature, and after the cracking temperature. An AFR of 120 mL min^{-1} was identified as the optimal level; exceeding or falling below this value inhibits the coal-oxygen reaction. Increasing OxyC and reducing HR improves coal oxidation. Compared to the same samples under AFR and HR conditions, the E_a of coal under oxygen conditions is lower, ranging between 20 and 35 kJ mol^{-1}, while under AFR and HR conditions, the E_a is not less than 30 kJ mol^{-1}, indicating a stronger tendency for spontaneous combustion under oxygen conditions. AFR substantially affects the oxygen consumption rate, CH_4, and exothermic intensity at all stages, with a partial η^2 of 0.6. Before the critical temperature, OxyC has the greatest impact on CO_2; between the critical temperature and the cracking temperature, OxyC has the greatest impact on CO; and after the cracking temperature, OxyC has the greatest impact on CO, CO_2, C_2H_4, and C_2H_6, with partial η^2 values of 0.51, 0.59, 0.278, and 0.45, respectively.

Keywords Characteristic temperature · Index gas · Apparent activation energy · Coal-oxygen reaction · Exothermic intensity

Introduction

Coal plays a dominant role in global energy production a situation expected to continue for some time [1, 2]. Coal mines present a unique set of hazards, particularly in the form of coal spontaneous combustion (CSC). Spontaneous combustion leads to fires or explosions, and poses a serious threat to the lives of miners, plant machinery, natural resources, and in some cases nearby communities. This adversely impacts productivity, the economy, and the environment [3, 4]. Coal mine goaf environments are complex, and the oxidation process during CSC can be affected by numerous factors, such as airflow rate (AFR), oxygen concentration (OxyC), and heating rate (HR).

Scholars have extensively examined the impact of external factors on the CSC process. Xia et al. [5] found that adjusting ventilation volume effectively inhibited gas from overrunning at the working face, forestalling CSC in high gas mines. As suggested by Yuan and Smith [6], ventilation caused heat loss during CSC, and so there was an optimal ventilation rate. Yang et al. [7] demonstrated that the risk area of a composite gas-and-CSC disaster was positively

✉ Jiajia Song
  songjiajia07@sina.com

[1] School of Safety Science and Engineering, Xi'an University of Science and Technology, Xi'an 710054, China

[2] Shaanxi Key Laboratory of Prevention and Control of Coal Fire, Xi'an 710054, Shaanxi, China

[3] Department of Safety, Health, and Environmental Engineering, National Yunlin University of Science and Technology, Yunlin, Taiwan 64002

correlated with air volume. Zhao et al. [8, 9], and Zhang et al. [10] showed that oxygen-poor conditions moderated CSC reaction intensity, such that as OxyC decreased, the coal E_a also decreased. As indicated by Zhou et al. [11], when OxyC increased, the overall change of gaseous products gradually increased. Lü et al. [12] reported that the critical pre-oxidation temperature of a pre-oxidised coal sample decreased when OxyC increased.

Ren et al. [13], Xiao et al. [14], and Zhong et al. [15] employed a C80 micro-calorimeter to measure the low-temperature oxidation heat-flow of pulverised coal samples. They found that the heat flow curve at a low OxyC clearly lagged behind. In addition, heat release decreased as OxyC decreased, but the characteristic temperature increased; this led to a reduction in the coal's microstructural functional groups. Perdochova et al. [16] looked into the effect of OxyC on gaseous products, during coal-self heating. Shen et al. [17] investigated bituminous coal and lignite separately. According to their study, within a certain range, the ignition point of coal undergoes an obvious decrease, as OxyC increases; at the same time, the authors also show E_a increases as OxyC increases, when the ignition temperature of the sample has been exceeded. Wang et al. [18] measured coal low-temperature oxidation under varying OxyC and methane conditions. They found that as OxyC increases, the influence of methane concentration on CSC is curtailed. Wen et al. [19] designed and manufactured a high-temperature CSC experimental device, and then conducted temperature-programmed experiments with different OxyCs. A variation in CSC characteristics was observed, and this provides a theoretical basis for the formulation of current fire prevention schemes.

Song et al. [20], Liu et al. [21], Zhai et al. [22], and Yang et al. [23] delved into the influence of HRs on CSC parameters. They showed that lower HRs could enhance the oxidation and heat release performance of coal, rendering the CSC heat release process more thorough. Zhang et al. [24] applied thermogravimetric analysis/differential scanning calorimetry-Fourier transform infrared spectroscopy (TGA/DSC-FTIR) coupling to explore the CSC process further. The authors found that as HR increased, the temperature of the exothermic zone also increased and that this delayed the release of CO and CO_2. Li et al. [25] and Onifade et al. [26] probed mass change during CSC, by conducting a thermogravimetric experiment. They found that both the exothermic reaction rate and mass-loss rate were larger at lower HRs. At higher HRs, the impacts of oxidative decomposition and gas phase combustion on mass-loss were diminished, whereas the solid-phase combustion effect increased. Guo et al. [27] used TGA to explore CSC characteristics. They discovered that HR was positively correlated with combustion reaction time, coal reaction rate, characteristic temperature, and oxidation rate.

In summary, previous studies often focused on the independent impact of a single external environmental factor on CSC characteristic parameters and only conducted qualitative studies on the effects of external factors on CSC. However, in the environment of goafs, the occurrence of CSC events is a complex process influenced by multiple factors, which significantly differs from the characteristics of CSC under a single external condition. Therefore, research on single factors needs to be supplemented by exploring the interactions and synergistic effects of multiple influencing factors, and it is necessary to quantitatively characterise their impact on CSC. This paper conducted an in-depth study of the low-temperature oxidation process of coal samples under different AFR, OxyC, and HR conditions through programmed temperature experiments. The experiments reveal the intrinsic relationships between gas release, heat generation, and temperature changes under these conditions. By examining the changes in the apparent activation energy (E_a) of coal samples, we further compared and analysed the influence of different external environments on CSC tendency. One-way analysis of variance quantitatively evaluated the significant impact of AFR, HR, and OxyC on CSC characteristic parameters. This study aims to provide a deeper understanding of the CSC mechanism, exploring ways to reduce or avoid the impact of CSC, and offering a scientific basis for the prevention and control of coal mine fires.

Experimental methods and theories

Coal sample preparation

Experimental coal samples were obtained from a southeastern Zhunnan coalfield, Xinjiang, China (Fig. 1). The high-quality humic coal from this region has a variety of industrial applications. After the coal sample was gleaned
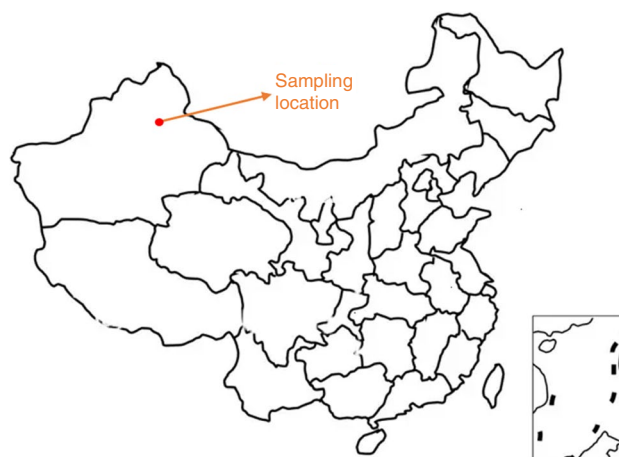

Fig. 1 Original sampling location

from the working face, it was sealed in a bag and transported to the laboratory, then crushed in ambient air. In accordance with GB/T477–2008, the coal samples were separated into the following particle sizes, 0–0.9, 0.9–3, 3–5, 5–7 mm, and the remainder were removed. Subsequently, 1 kg of the experimental coal sample (in a 1:1:1:1:1 mass ratio) was tested. A quality analysis of the coal sample is presented in Table 1.

Programmable isothermal oven experiment

A temperature-controlled, programmed heating device, as depicted in Fig. 2 [28], was utilised. The experimental coal sample was loaded into the tank, and its temperature was continuously monitored in real-time during the heating process. Gas chromatography (GC) was employed to assess the captured gas that was given off at various temperatures. The experiment commenced at room temperature, and at 30 °C, a GC analysis was conducted. Subsequently, gas samples were obtained at every 10 °C increment in coal temperature, up to and including 200 °C. In total, the gas analysis was performed 18 times. Once the heating process had concluded, the gas supply was shut off and the experiment was considered complete after the coal body had naturally cooled to room temperature. Detailed experimental conditions are presented in Table 2.

Table 1 Results of the proximate and ultimate analyses of coal samples

Proximate analysis		Elemental analysis	
Moisture content (%)	3.05	C (%)	63.25
Ash content (%)	17.49	H (%)	1.28
Volatile matter (%)	33.84	O (%)	3.76
Fixed carbon (%)	48.32	N (%)	1.25

Table 2 Experimental test conditions for the programmed-temperature rise of coal samples

Group number	AFR/mL min^{-1}	HR/°C min^{-1}	OxyC/%
1	40	0.3	21
2	80	0.3	21
3	120	0.3	21
4	160	0.3	21
5	120	0.3	21
6	120	0.4	21
7	120	0.5	21
8	120	0.6	21
9	120	0.3	3
10	120	0.3	7
11	120	0.3	10
12	120	0.3	15
13	120	0.3	21

Oxygen consumption rate

Because coal mainly reacts with O_2 in an oxidation reaction, the oxygen consumption rate can be computed by observation of the OxyC, and its tendency toward CSC can be determined. The oxygen consumption rate of the coal sample can be described by Eq. (1) [29]:

$$v(O_2) = \frac{Q \times C_{O_2}^1}{V} \ln \frac{C_{O_2}^1}{C_{O_2}^2} \tag{1}$$

where Q is the AFR in mL min^{-1}, V is the volume of the tank in cm^3, $C_{O_2}^1$, $C_{O_2}^2$ is the OxyC at the entrance, and $C_{O_2}^2$ is the OxyC at the exit, in mol cm^{-3}.

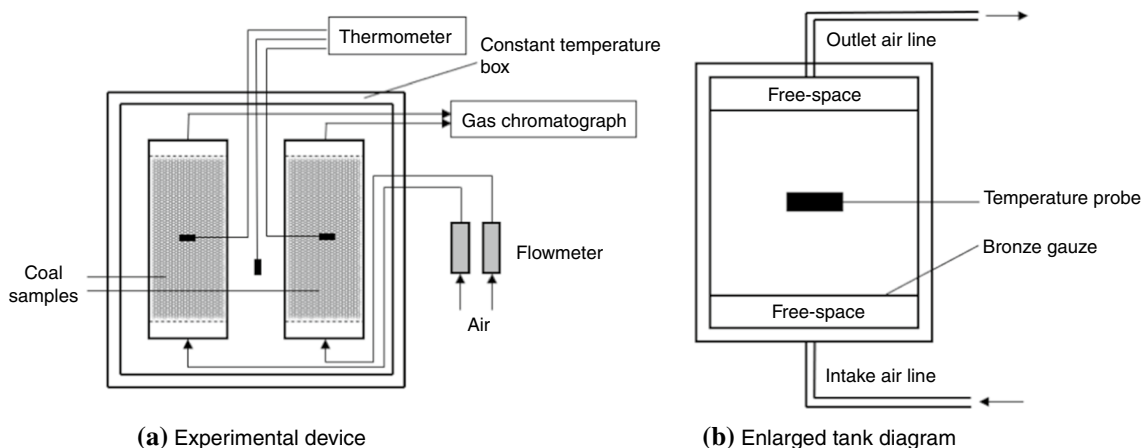**(a)** Experimental device **(b)** Enlarged tank diagram

Fig. 2 The devices used for the temperature programmed experiment. **a** The experimental device, and **b** an enlarged diagram of the tank

Exothermicity

Chemical bond energy conservation estimation was utilised to determine the exothermic intensity of the CSC event. That is, it was assumed that the oxygen consumed during CSC was entirely used to generate either CO, or CO_2 and heat. The exothermic intensity $q_{max}(T)$ is expressed by Eq. (2) [30, 31], which is the maximum exothermic intensity:

$$q_{max}(T) = \frac{V_{CO}^0(T)}{V_{CO}^0(T) + V_{CO_2}^0(T)} \cdot V_{O_2}^0(T) \cdot$$

$$q_{co} + \frac{V_{CO_2}^0(T)}{V_{CO}^0(T) + V_{CO_2}^0(T)} \cdot V_{O_2}^0(T) \cdot q_{co_2}$$

$$(2)$$

If the oxygen consumption is considered to be chemisorption, except for the generation of CO and CO_2, then the exothermic intensity $q_{min}(T)$ can be expressed by Eq. (3), which is the minimum exothermic intensity:

$$q_{min}(T) = q_a \cdot \left[V_{O_2}^0(T) - V_{CO}^0(T) - V_{CO_2}^0(T) \right]$$
$$+ V_{CO}^0(T) \cdot q_{co} + V_{CO_2}^0(T) \cdot q_{co_2}$$

$$(3)$$

where $V0\ CO_2(T)$ is the standard CO_2 production rate in mol $cm^{-3}\ s^{-1}$, $q\ CO_2$ and q_{co} are the reaction heat of the CO_2 and CO in kJ mol^{-1}, respectively, and $q_a = 58.8$ kJ mol^{-1} [31].

Apparent activation energy

The CSC process is a self-accelerating heating process, in which the functional groups reach their E_a and after which begin to react with oxygen. E_a refers to the minimum energy necessary for the decomposition of coal samples in the pyrolysis reaction. If the E_a is lower, the chemical reaction proceeds more readily, and the tendency toward CSC is higher. The reaction order was determined to be 1, following the principles of the Arrhenius equation, and the coal-oxygen reaction rate can be expressed as Eq. (4) [32]:

$$v(O_2) = A \cdot C_{O_2}^1 \cdot e^{-\frac{E_a}{RT}} \tag{4}$$

where A is the pre-exponential factor, E_a is the apparent activation energy in J mol^{-1}, R is the gas constant in 8.314 J $mol^{-1}\ K^{-1}$, and T is the thermodynamic temperature of coal in K, $C_{O_2}^1 = 9.375 \times 10^{-6}$ mol cm^{-3}. Equation (4) is log-transposed and expressed as shown in Eq. (5):

$$\ln \frac{v_{O_2}}{C_{O_2}^1} = \ln A - \frac{E_a}{R \cdot T} \tag{5}$$

Equation (5) describes a linear correlation between $\ln[v\ O_2/C1\ O_2]$ and $1/T$, allowing for the calculation of E_a through its slope $-E_a/R$.

Results and analysis

Oxygen concentration

The experimental results showing the change in O_2 concentration during CSC are illustrated in Fig. 3. Below 70 °C, the O_2 concentration decreases slowly and is almost stable. During that period, the main reason for the decrease in oxygen is adsorption by the coal sample. Between 70 and 130 °C, a minute amount of active functional groups begins to participate in the oxidation reaction, which leads to a decrease in O_2 concentration. After 130 °C, the O_2 concentration decreases rapidly, and the alternation range is higher than the previous change range. Thus, as the number of active functional groups increases, the oxidation rate also increases rapidly.

When the temperature was held constant and AFR increased, the O_2 concentration remained low when the AFR was 120 mL min^{-1}. However, with an AFR of 160 mL min^{-1} and a temperature above 80 °C, the O_2 concentration gradually decreases, compared to the O_2 concentration at 40 and 80 mL min^{-1}. Despite the above-mentioned, the concentration is only slightly higher than the corresponding O_2 concentration for an AFR of 120 mL min^{-1}. At lower temperatures, the heat generated in the coal oxidation process is lower than the heat taken away at higher AFRs, which hinders the reaction.

For varying HRs, above 100 °C, when the HR is 0.3 °C min^{-1}, the concentration of O_2 remains low. For HRs 0.4, 0.5, and 0.6 °C min^{-1}, the O_2 concentration is around 10%, but it first reaches the previous value at the HR of 0.4 °C min^{-1}. At an HR of 0.3 °C·min^{-1}, the concentration of O_2 first increases slightly and then decreases swiftly, eventually reaching around 2%. The main reason may be that when the HR becomes smaller, it takes longer for the HR to reach the same temperature, and so the coal itself is given more time to store the heat. When the HR is greater than 0.4 °C min^{-1}, the heat generated is similar to the heat taken away by the air, leading to less heat storage. Moreover, the failure to reach the energy required for activation of the active functional groups results in a stable O_2 concentration. The heat storage under an HR of 0.3 °C min^{-1} is relatively large, but the conditions for an oxidation reaction for some functional groups were reached after some period of time. This is demonstrated by a swift decrease in O_2 concentration after the rebound in the figure. When the initial OxyC is higher, more oxygen is consumed during the experiment. Despite this, when
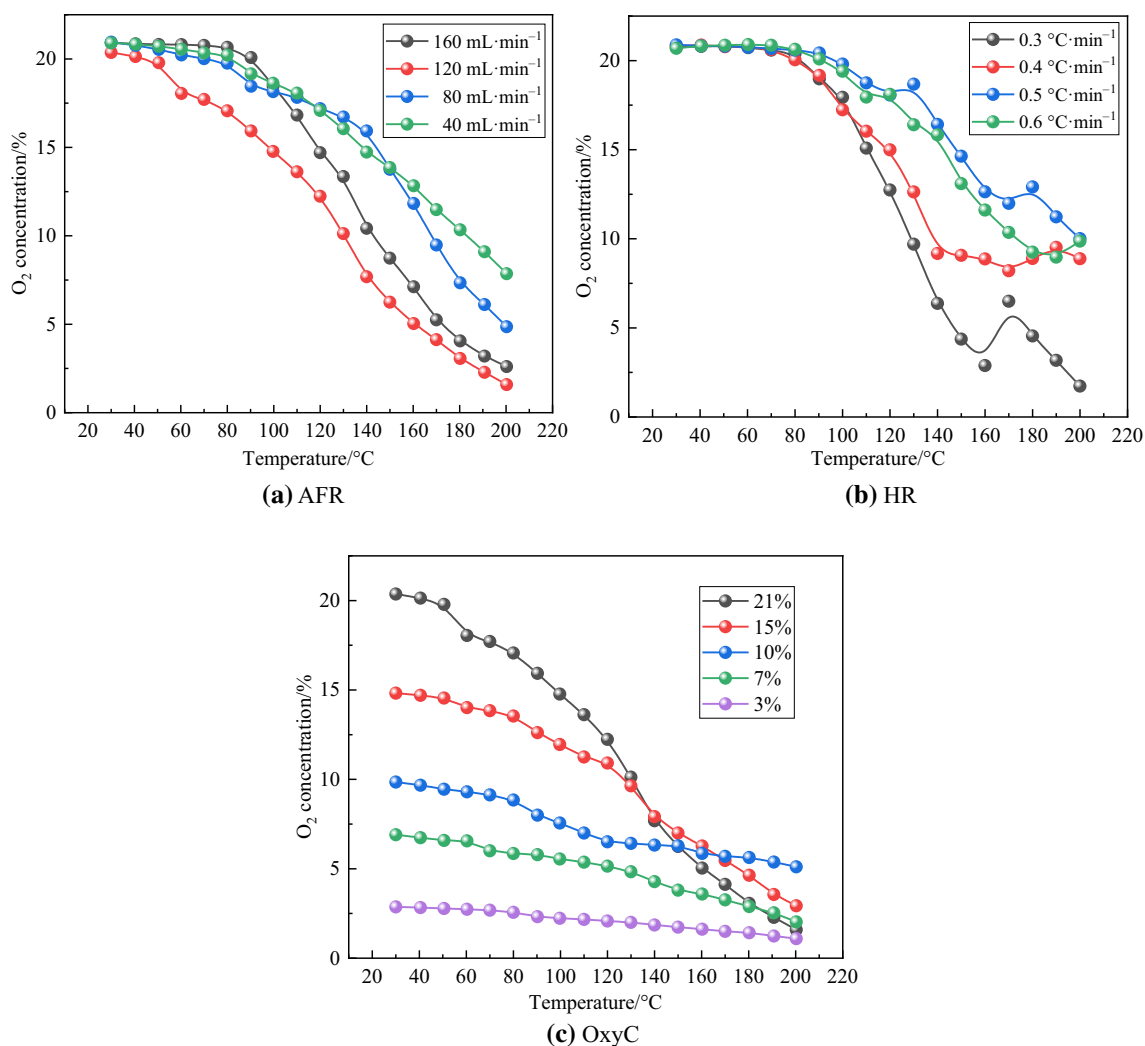
(a) AFR

(b) HR

(c) OxyC

Fig. 3 O_2 concentration curves for different temperatures under multivariate conditions for, **a** AFR, **b** HR, and **c** OxyC

the temperature exceeds 120 °C, the slope of the curve is the smallest at 10% OxyC, and so the decrease in the O_2 concentration is the slowest.

Oxygen consumption rate

Figure 4 illustrates the variations in the oxygen consumption rates of the coal samples, as calculated using Eq. (1). Under different conditions, the oxygen consumption rate exhibits a positive correlation with temperature increase. Up to 70 °C, the oxygen consumption rate displays a gradual change. This is mainly influenced by the sample's inherent oxygen absorption rate, and the compound rate of coal and oxygen. In the range of 70−130 °C, a first mutation occurs, and a gradual increase in the oxygen consumption rate is observed. This is mainly due to the enhanced chemical reaction rate between the sample and oxygen, which is a result of the elevated temperature. Beyond 130 °C, a second mutation

is observed, thereby leading to a sharp rise in the oxygen consumption rate.

When the temperature was held constant, the oxygen consumption rate first increased and then decreased as AFR increased. The oxygen consumption rate was the greatest when the AFR was 120 mL min^{-1}, and the oxygen consumption rate was least when the AFR was 40 mL min^{-1}. This is because the AFR of 160 mL min^{-1} caused excessive heat dissipation, hindering the reaction process and leading to a lower oxygen consumption than under the AFR of 120 mL min^{-1}.

When the HR was varied, the curve changes were similar for the 0.4, 0.5, and 0.6 °C min^{-1} HR experiments. The oxygen consumption rate tended to be ca. 1100×10^{-11} mol cm^{-3} s^{-1}. Under an HR of 0.3 °C min^{-1}, the oxygen consumption rate decreased slightly and then increased quickly, finally reaching around 3700×10^{-11} mol cm^{-3} s^{-1}. This corresponds to changes in
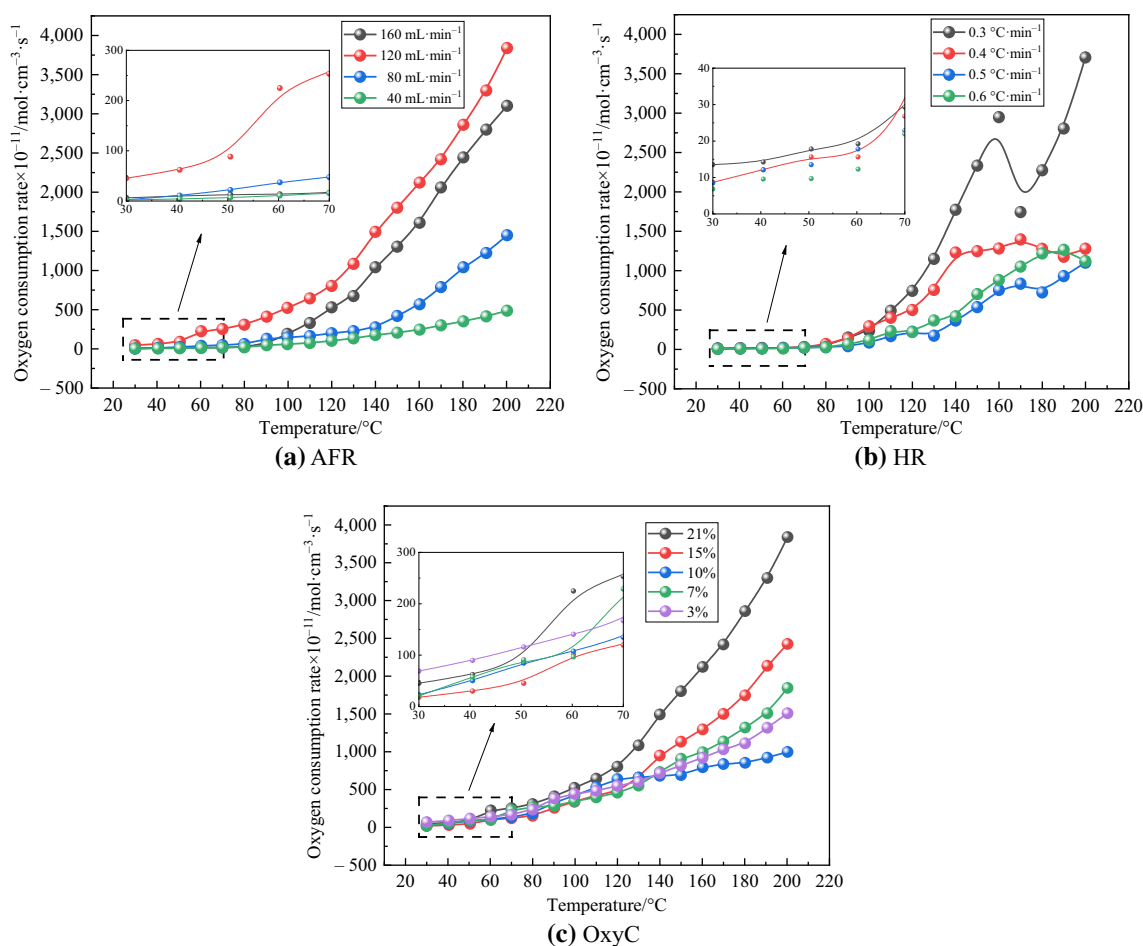
Fig. 4 Oxygen consumption rates curves for different temperatures under multivariate conditions for, **a** AFR, **b** HR, and **c** OxyC

the O_2 concentration. Specifically, if the temperature was less than 130 °C, the oxygen consumption rate increased as OxyC increased. When the temperature exceeded 130 °C, the oxygen consumption rate curve did not change prominently, at 10% OxyC. This led to a slow increase in the oxygen consumption rate, which was lower than for other OxyCs.

Figure 4c shows the impact of an oxygen-deficient environment on CSC. Before 70 °C, there is no prominent difference in the oxygen consumption rate under different OxyC levels. However, under 21% OxyC, the oxygen consumption rate first changes abruptly around 50 °C and remains the highest at the same temperature thereafter. This indicates that once the coal-oxygen composite reaction commences, the low-temperature oxidation rate of coal under 21% OxyC is faster compared to other oxygen-deficient conditions. Therefore, 21% can be considered the optimal OxyC for CSC. This conclusion is consistent with the findings of Ren [33] et al. for bituminous coal. Between 70 and 130 °C, except for another abrupt change in the oxygen consumption rate at 120 °C under

21% OxyC, the oxygen consumption rates under other oxygen-deficient conditions exhibit a slow increasing trend. Notably, under 10% OxyC, the rate of oxygen consumption slows after 120 °C, gradually lagging behind other OxyC conditions until the end of the experiment. When the temperature exceeds 130 °C, the impact of the oxygen-deficient environment on the oxygen consumption rate becomes exceptionally apparent. Except for 10% OxyC, the oxygen consumption rate increased with the increase in OxyC, indicating that increasing OxyC positively promoted the CSC process. These observations are generally consistent with the research of Yan et al. [34] and Wen et al. [19], who found that under different oxygen-deficient conditions, the oxygen consumption rates of anthracite and long-flame coal increase with the increase in OxyC. They also note that the increase in OxyC promotes oxidation reactions, with the extent of OxyCs influence varying at different temperatures.

In general, the oxygen consumption rate increased from 45×10^{-11} mol cm^{-3}·s^{-1} at the initial temperature, to 225×10^{-11} mol cm^{-3}·s^{-1} at an AFR of 120 mL min^{-1}

AFR, up to 70 °C. The oxygen consumption rate fluctuated slightly at other AFRs and different HRs, but the changes did not exceed 20×10^{-11} mol cm^{-3} s^{-1}. The oxygen consumption rate increased at different OxyCs, and reached 100×10^{-11} mol cm^{-3} s^{-1}, except for 21% OxyC, which was 225×10^{-11} mol·cm^{-3} s^{-1}. Between 70 and 130 °C, a higher oxygen consumption rate became visible, particularly under AFRs 160, 120 and 80 mL min^{-1} AFR, and for HR of 0.3 and 0.4 °C min^{-1}; however, the oxygen consumption rate did not increase noticeably under other HRs. It reached 1050×10^{-11} mol cm^{-3} s^{-1} at 21% OxyC, but only increased a little under other OxyC conditions. At this time, the AFR was observed to have a substantial influence on heat dissipation during sample oxidation, indicating that the heat storage conditions of coal had a remarkable influence on progression of the oxidation process.

When the temperature exceeded 130 °C and the AFR was 80 mL min^{-1}, the oxygen consumption rate started to increase noticeably. Except for an HR of 0.3 °C min^{-1}, oxygen consumption was stable, reaching around 1150×10^{-11} mol cm^{-3} s^{-1}. The oxygen consumption rate of various OxyCs launched demonstrated a substantial gap. This showed that the change in heat production, caused by the change in HR, was smaller than the amount of heat taken removed by the AFR. Meanwhile, the demand for oxygen increased due to the violent oxidation reaction at this time.

Characteristic temperature

The characteristic temperature of the sample was appraised using the index gas growth rate method, as shown in Eq. (6) [35]:

$$Z = \frac{C_{i+1} - C_i}{C_i \cdot (T_{i+1} - T_i)} \qquad (6)$$

where Z is the overall growth rate of the index gas volume fraction, C_i and C_{i+1} are the volume fractions of gas at a given point in time, and the subsequent point, respectively, and T_i and T_{i+1} are the temperatures at a given point in time, and the subsequent point, respectively, in °C.

Taking CO as the main index gas of CSC [36, 37], the change law of its growth rate was analysed to determine the characteristic temperature of the sample. The change in CO growth rates is illustrated in Figs. 5–7.

Figures 5–7 exhibit that the CO concentration increased as the temperature increased, across the various experimental conditions; the higher the temperature, the faster the increase in CO concentration. The index gas growth percentage analysis shows that the CO growth percentage curve reaches a peak, and the temperature corresponds to the characteristic temperature point of the coal sample. From the growth percentage curve, it is observed that when the curve reaches its first peak, it then decreases rapidly, and quickly returns to find a second peak. The CO concentration curve shows that the CO concentration increases near to the first peak temperature. After the temperature rises to ~ 90 °C, the hyperoxide in the coal starts to decompose [38]. This produces an enormous amount of CO, and so, leading to the second curve peak.

When the CO growth curve reaches its third peak, it changes abruptly, showing a sharp increase. This is the cracking temperature, and as the temperature continues to increase, the more stable functional groups begins to actively participate in the reaction. There is variance in the amount of CO produced at given temperatures, owing to the different functional groups activating at different temperatures, but these peaks are observed above the cracking temperature.

In summary, the critical temperature of the sample was between 65 and 75 °C. The cracking temperature was in the range 115–130 °C. Thus, the CSC process exhibits three stages: Stage 1, pre-critical temperature; Stage 2, interim, between critical temperature and dry cracking; and Stage 3, post-cracking.

Carbon–oxygen gases

CO release phenomena

Figure 8 shows the exponential increase in the CO concentration under various conditions within the temperature range of 30–200 °C. In Stage 2, when the internal structure of the coal loosens, the increase in CO concentration is due to the physical adsorption of oxygen within the coal pores [39]. After Stage 3, a large amount of oxygen is adsorbed by the coal body, and the CO concentration increases sharply, indicating that the coal could enter rapid oxidation. At that time, the oxygen is mainly supplied by chemisorption, which is consistent with prior research [40–45].

When the AFRs are 120 and 160 mL min^{-1}, the CO concentrations are similar. The CO concentration is lowest when the AFR is 40 mL min^{-1}. As the temperature increases, the CO concentration at 120 mL min^{-1} AFR gradually exceeds the corresponding CO concentration at 160 mL min^{-1}. At this time, the reaction is sufficient, and the excess air reduces some of the accumulated heat, hindering the reaction. The excess O$_2$ reacts with the CO to form CO$_2$, resulting in lower CO concentrations [46].

When examining HR effects, in general, CO is generated slowly prior to Stage 3. During Stage 3, CO concentrations increases exponentially; at temperatures above 180 °C, a lower HR results in a greater gas concentration. Here, 21% OxyC produces the greatest concentration of CO. As OxyC increases, CO concentration increases for tests at the same HR. This is because when the OxyC increases, this provides the active functional groups with
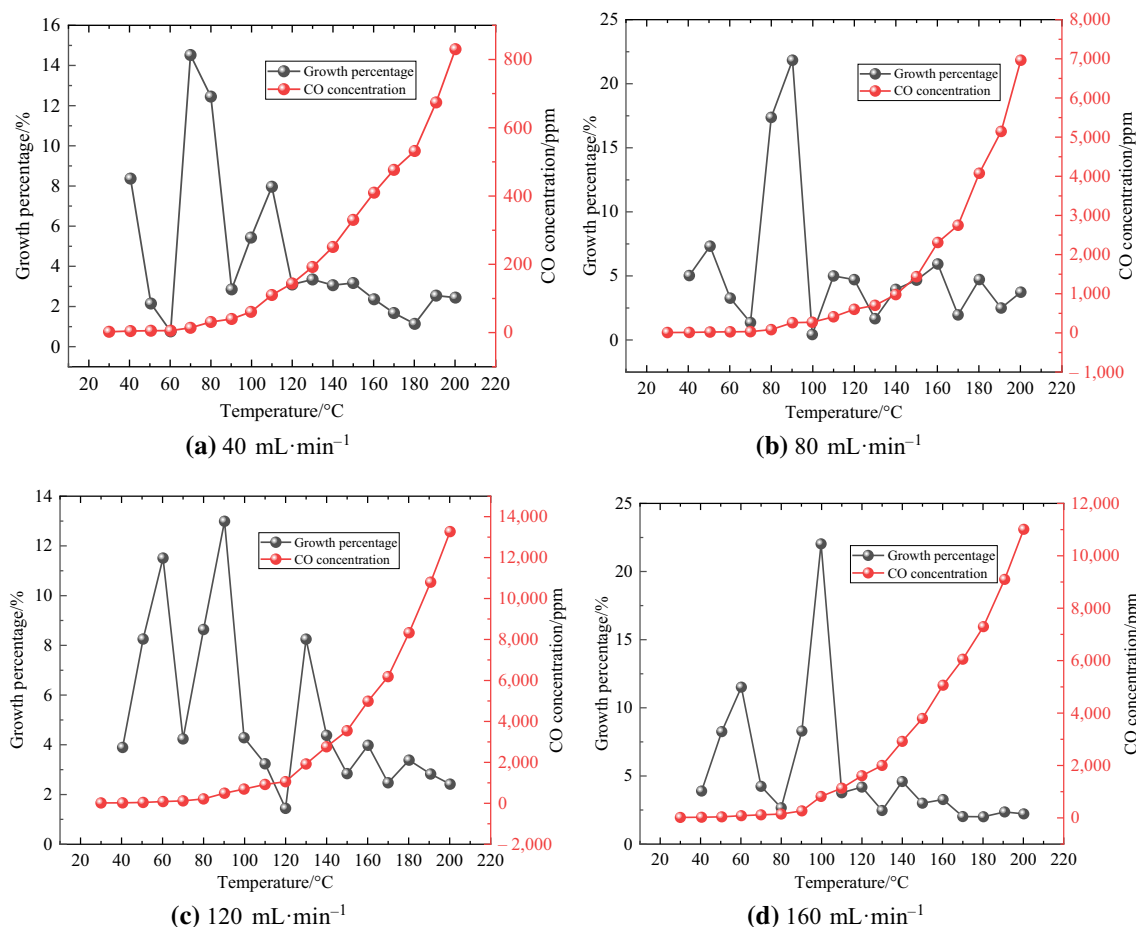
Fig. 5 CO concentration curves and their growth percentages at different temperatures, and under AFRs of **a** 40 mL min^{-1}, **b** 80 mL min^{-1}, **c** 120 mL min^{-1}, and **d** 160 mL min^{-1}

an opportunity to react with the oxygen, leading to a greater gas yield. Here, 10% OxyC produces a relatively stable concentration of CO, showing that limiting OxyC to 10% can inhibit CSC, to a certain extent. However, the oxidation process cannot be entirely prevented [46].

The CO concentration curves for AFRs of 120 and 160 mL min^{-1} in Stage 1 occur after almost the same time interval. These data are clearly different the 40 and 80 mL min^{-1}AFR data. At different HRs, the CO concentrations are similar below 60 °C, and the observed differences gradually appear after 60 °C. Despite the above-mentioned, it still maintains relatively synchronous growth patterns for HRs of 0.3, 0.4, 0.5, and 0.6 °C min^{-1}, respectively. The difference in CO concentrations under different OxyC conditions is readily apparent.

After Stage 1, under various AFRs, the different CO concentrations gradually become apparent. However, the 120 and 160 mL min^{-1} AFRs remain comparable. The difference in CO concentrations under HR changes remains small. However, the difference in CO concentrations under

different OxyCs shows an increasing trend. This indicates that OxyC not only determines coal oxygen reaction efficiency but also affects CO production efficiency. Because the production of CO is closely related to –C=O and –CHO [38], different OxyCs have a considerable influence on the activity involved in these two groups. Thus, as the OxyC increases, the activity in these two groups, as functional groups, becomes greater.

CO$_2$ release phenomena

CO$_2$ release findings are consistent with the CO findings. They increase exponentially as temperature increases. The findings in this paper are consistent with those of Zhao et al. [47], and Niu et al. [48]. As shown in Fig. 9, CO$_2$ is detected in all samples immediately after the experiment is conducted. The concentrations are large, at least twice the concentration of CO. Owing to the large molecular mass of CO$_2$, a large amount of CO$_2$ is adsorbed by the coal macromolecules due to the van der Waals force. When
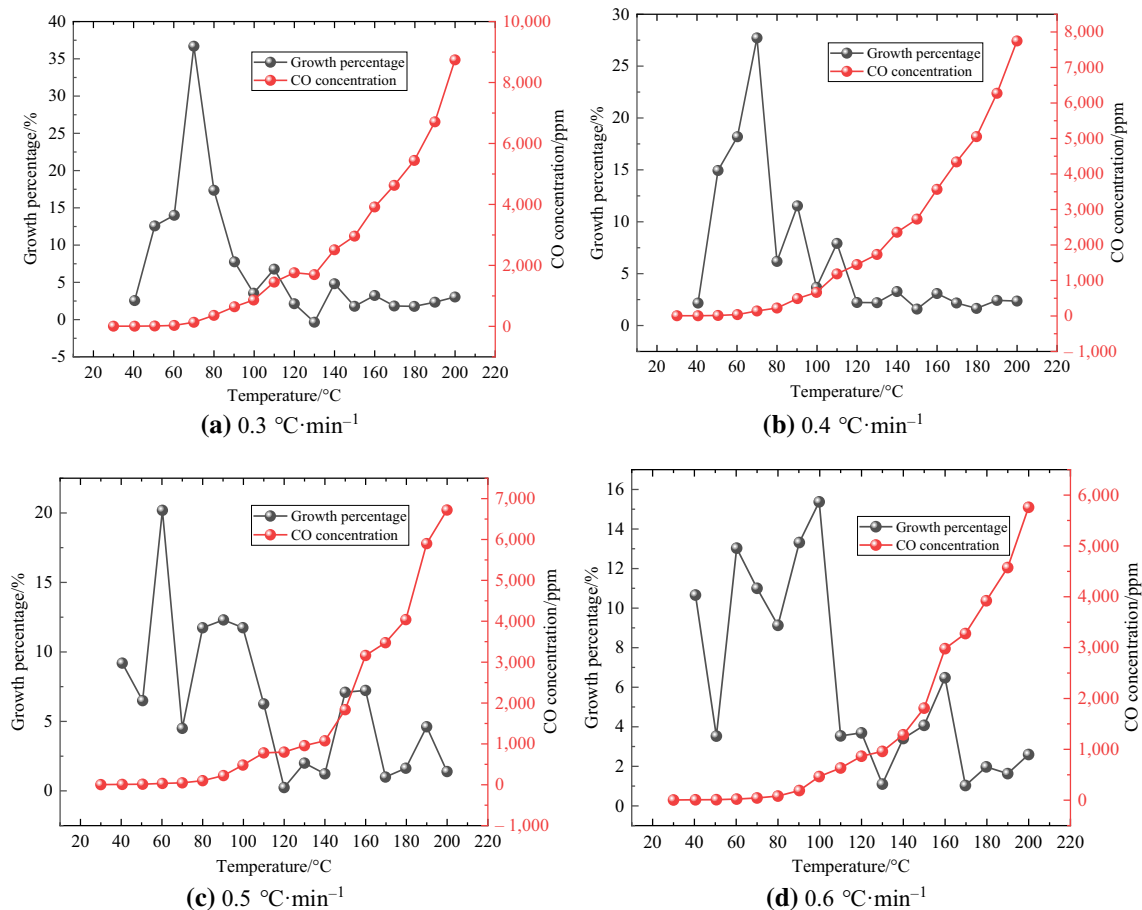
Fig. 6 CO concentration curves and their growth percentages at different temperatures, and under HRs of **a** 0.3 °C min^{-1}, **b** 0.4 °C min^{-1}, **c** 0.5 °C min^{-1}, and **d** 0.6 °C min^{-1}

the temperature increases, the CO_2 gradually desorbs, and so a small part of the water oxygen complex is converted into CO_2. In addition, the increase in C=O content leads to an increase in the number of carboxyl groups and the release of CO_2 [43].

When varying the AFR, the CO_2 concentrations remain similar. The highest concentration is observed under an AFR of 120 mL min^{-1} in Stage 3. When the HR was different, the production of CO_2 was relatively slow before Stage 3. In Stage 3, the concentration of CO_2 increases exponentially. When OxyC varies, the concentration of CO_2 increases as OxyC increases, up to 110 °C, although the corresponding CO_2 concentration at 10% OxyC does not show any notable change. At 10% OxyC, CO_2 concentrations are the lowest, but still show an increasing trend. This is because the CO_2 generation pathway is more than CO, and some CO also reacts to generate CO_2, causing the CO_2 concentration to substantially increase after the drying temperature.

The CO_2 concentration curves that correspond to the 120 and 160 mL·min^{-1} AFRs below 50 °C are overlapped before the critical temperature is reached. The CO_2 concentration curves corresponding to the 40, 120, and 160 mL min^{-1} AFRs above 50 °C are exceptionally similar. When the HR is 0.3 °C·min^{-1}, there is little difference in the CO_2 concentration below 40 °C at 0.5 °C min^{-1}. After 40 °C, it is similar to the corresponding concentration of CO_2 at the HR of 0.4 and 0.6 °C min^{-1}. Varying the OxyC produces CO_2 concentration curves that have no crossover points, and a higher OxyC corresponds to a higher CO_2 concentration. After Stage 1, the gap between the CO_2 concentration curves gradually increases, in line with increasing OxyC, whereas the CO_2 concentration curves remain relatively similar under different AFR and HR conditions. The reaction of the coal molecules with oxygen to form CO_2 is complete, and the OxyC has a notable influence on the production of CO_2. As documented in the existing literature, there are several ways that CO_2 can be generated. For example, the –COOH, –C = O, –CHO, and –OH groups are closely related to CO_2 [48, 49]. Accordingly, OxyC could have a considerable influence on the activity of these four functional groups, and the higher the OxyC, the greater the activity of the functional groups.
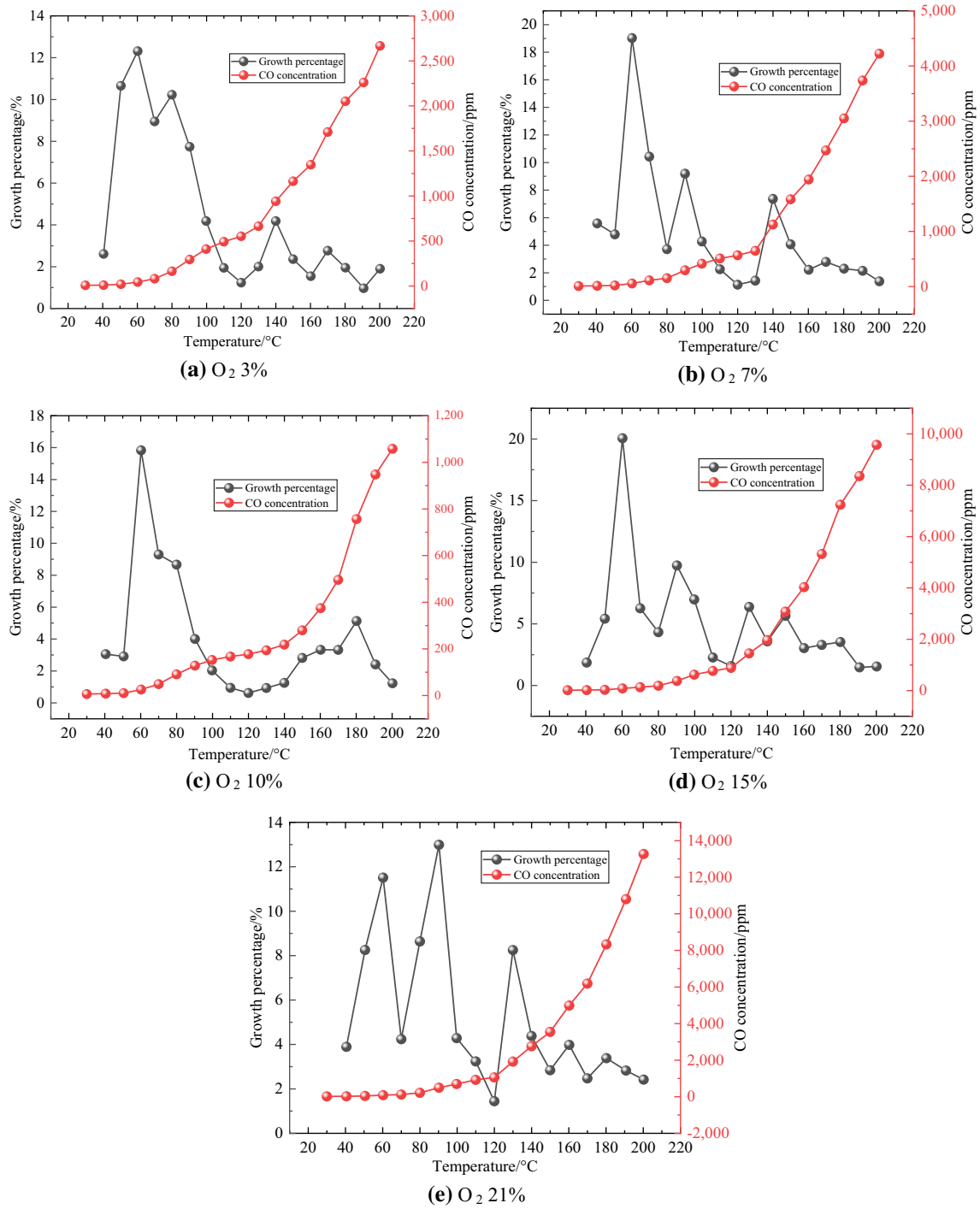
Fig. 7 CO concentration curves and their growth percentages at different temperatures, under OxyCs of **a** O$_2$ 3%, **b** O$_2$ 7%, **c** O$_2$ 10%, **d** O$_2$ 15%, and **e** O$_2$ 21%
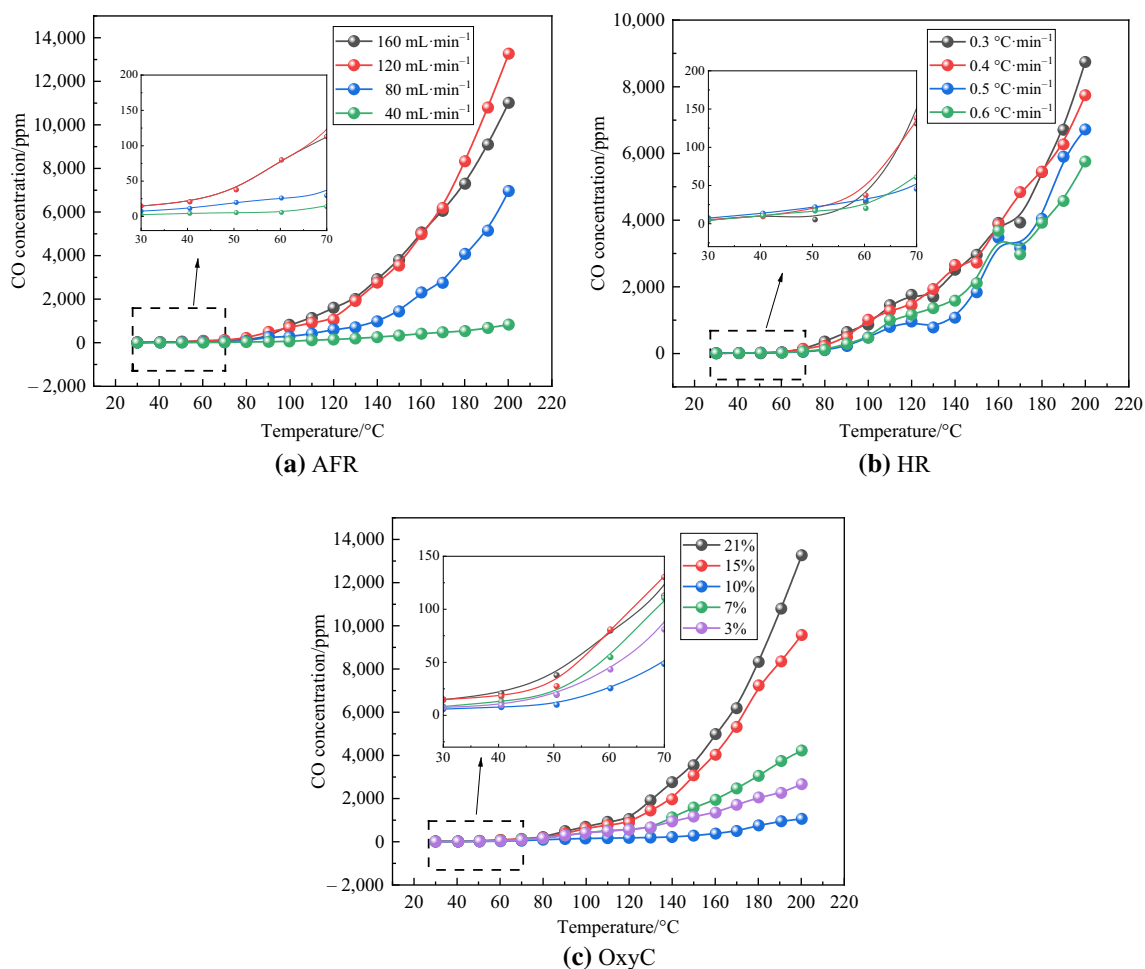
Fig. 8 CO concentration curves at different temperatures, under multivariate conditions for **a** AFR, **b** HR, and **c** OxyC

Hydrocarbon gases

CH₄ release phenomena

CH_4 is a primary hydrocarbon gas that can be readily detected. This is also one of the main gaseous products of oxidative coal pyrolysis. As depicted in Fig. 10, a limited quantity of CH_4 is generated in the initial stage of the experiment. This is because the coal itself contains a certain amount of CH_4 that exists in either free or adsorbed states. At that stage, CH_4 is released through the desorption of gas that had previously been adsorbed on the coal surface. Afterwards, the gas concentration increases promptly as the coal-oxygen reaction intensifies. Zeng and Shen [50] obtained the same research results. From a microscopic perspective, as the oxidation temperature increases, the CH_4 adsorbed on the coal surface desorbs and releases CH_4. In addition, the reaction of lipid compounds in the coal molecules also releases CH_4 [47].

When varying the AFR, CH_4 concentration is first observed to increase and then decrease as AFR rises for the same temperature. The observed CH_4 concentrations are highest for 120 mL min⁻¹ AFR. When varying the HR, CH_4 concentration decreases in the physical adsorption stage. After Stage 1, the curves corresponding to 0.3 and 0.4 °C min⁻¹ are quite different from the 0.5 and 0.6 °C min⁻¹ curves. When the temperature reaches 200 °C, the CH_4 concentration for HRs 0.4, 0.5, and 0.6 °C min⁻¹ is roughly the same, approximately 250 ppm. In contrast, the CH_4 concentration produced at 0.3 °C min⁻¹ is ca. 330 ppm. Except under a 10% OxyC, the CH_4 concentration decreases as OxyC decreases for the same temperature. A 10% OxyC inhibits the formation of aromatic hydrocarbons [46], and this also partially inhibits the coal oxidation reaction. Aromatic hydrocarbons are one of the main sources of hydrocarbon gases, so the CH_4 concentration increases slowly.

In Stage 1, because the CH_4 is mainly desorbed from the CH_4 on the coal surface, the difference in the CH_4 concentration curves under different experimental

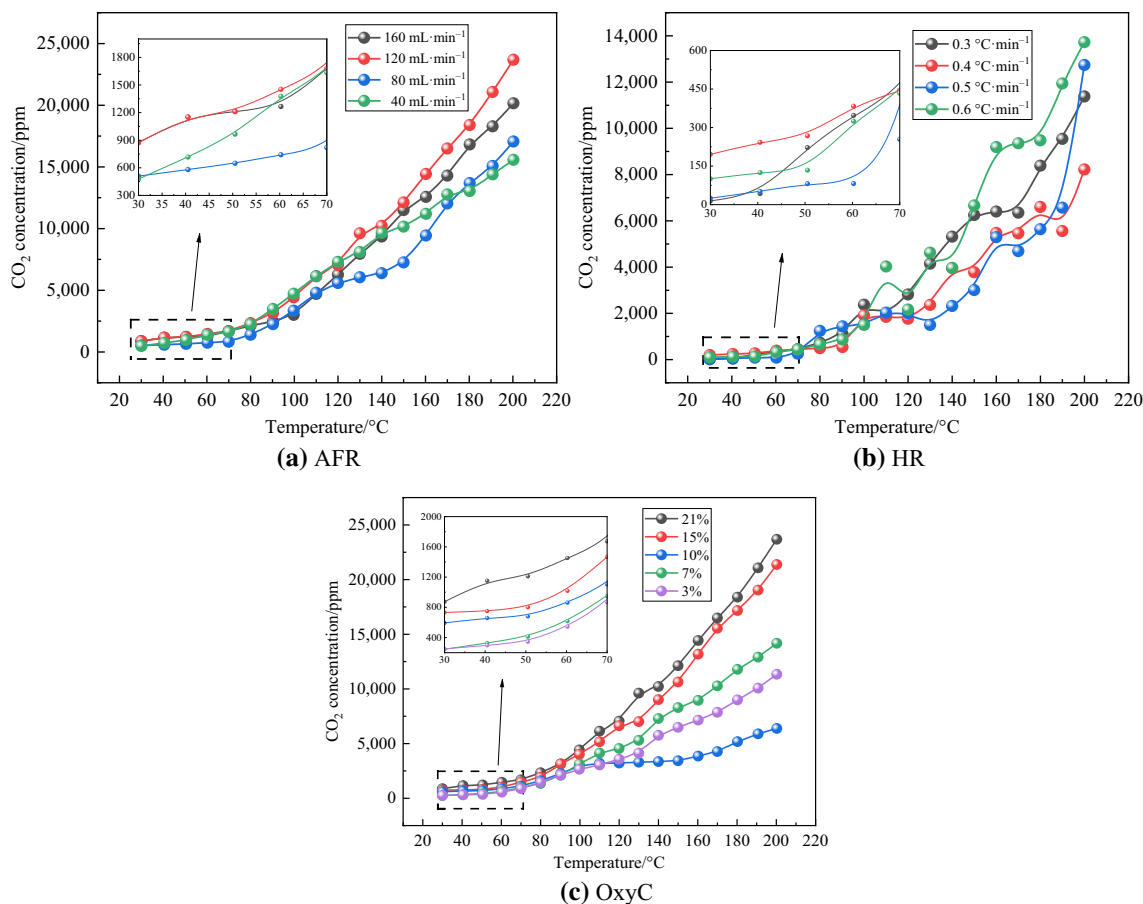**Fig. 9** CO_2 concentration curves at different temperatures, under multivariate conditions for **a** AFR, **b** HR, and **c** OxyC

conditions is small. In Stage 2, the CH_4 concentrations are remarkably different for different AFRs. The CH_4 concentrations are similar, below 90 °C, for different HRs. After the temperature exceeds 90 °C, the CH_4 concentrations under HRs 0.5 and 0.6 °C min^{-1} show no pronounced difference. The CH_4 concentration is 10 to 43 ppm below 120 °C at 3%, 7%, and 15% OxyCs. The difference in CH_4 concentrations over the holistic process is slightly lower, and so the curve has more intersection points. From this, it can be concluded that the AFR has a greater impact on CH_4, at this stage. In Stage 3, except for AFRs of 80 and 160 mL min^{-1}, the curves are relatively close after 160 °C; although there is a clear gap in the CH_4 concentrations under different AFRs.

The CH_4 concentration curves at different HRs follow the trends of the previous stage. The CH_4 concentration curves under different OxyCs show a distinct hierarchy, indicating that oxygen has an increasing effect on CH_4 generation. The influence of AFR on the generation of CH_4 is less, but still noticeable. Therefore, both OxyC and

AFR have a greater impact on the concentration of CH_4. In Stage 3, because of the strong correlation between the CH_4, $-CH_2-$, and $-CH_3$ groups [46], different AFRs affect the activity in these two groups as functional groups. Thus, under an AFR of 120 mL min^{-1}, the effects are more pronounced.

C_2H_4 and C_2H_6 release phenomena

As shown in Figs. 11 and 12, the C_2H_4 and C_2H_6 concentrations manifest a positive correlation with increasing temperatures across different conditions. The C_2H_4 and C_2H_6 concentrations are first detected in the samples under different conditions between 90 and 120 °C, indicating that they are high-temperature reaction products. Other scholars [51, 52] have obtained the same results. As the temperature increases, the aliphatic hydrocarbons in the free phase of coal, including the aliphatic side chains on the aromatic ring, crack gradually, thereby producing C_2H_4 and C_2H_6 via free
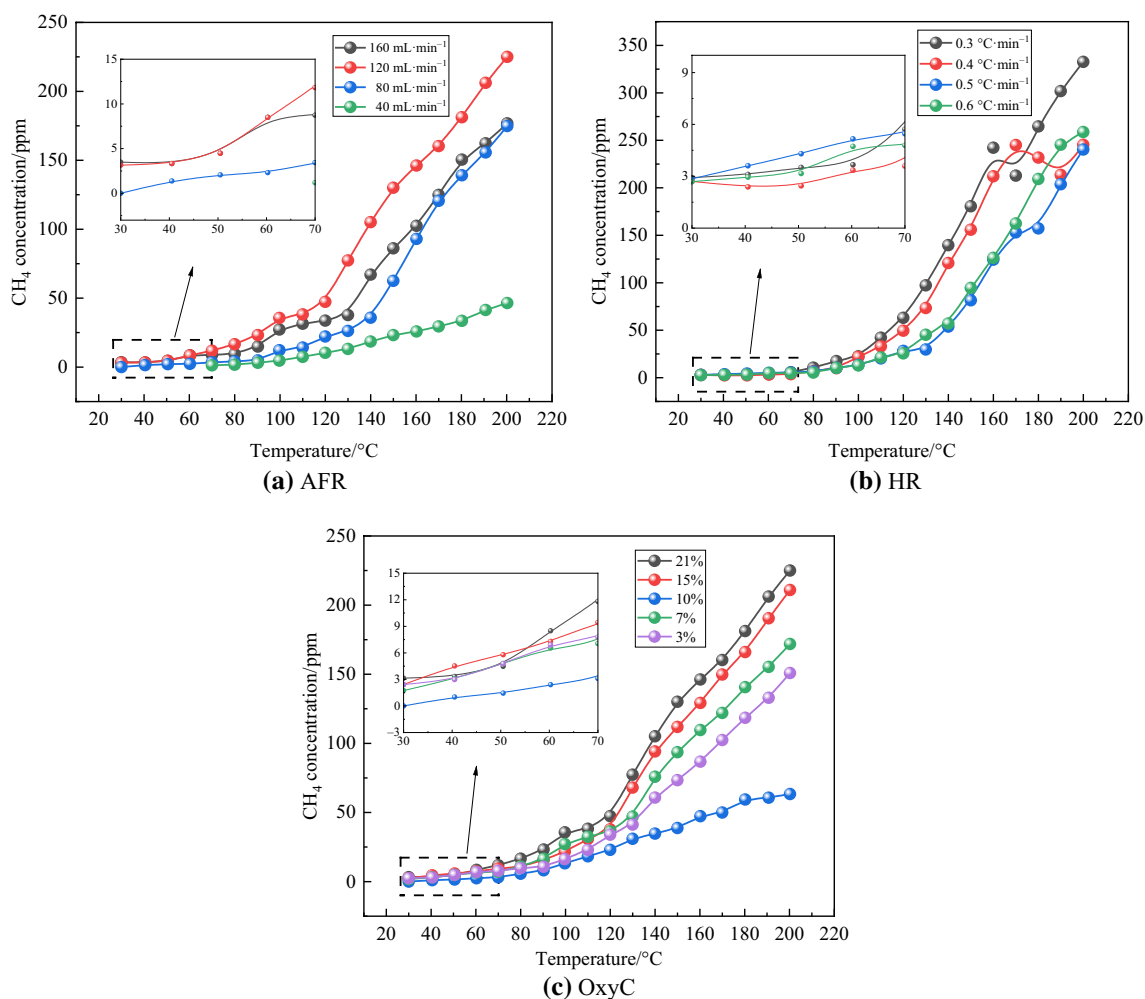
Fig. 10 CH$_4$ concentration curves at different temperatures, under multivariate conditions for **a** AFR, **b** HR, and **c** OxyC

radicals [53]. As C$_2$H$_6$ is more stable than C$_2$H$_4$, a greater amount of C$_2$H$_6$ is produced, at the same temperature.

When the AFR is 120 mL min^{-1}, C$_2$H$_4$ is first detected at 100 °C, but C$_2$H$_6$ is detected at 90 °C. At the same temperature, the C$_2$H$_4$ and C$_2$H$_6$ concentrations under an AFR of 120 mL min^{-1} are the largest, and an AFR of 40 mL min^{-1} yields the least. These results remain consistent. When HR varies, C$_2$H$_4$ and C$_2$H$_6$ are first detected at 90 °C under an HR of 0.3 °C min^{-1}. At an HR of 0.6 °C·min^{-1}, the minimum detection temperature of C$_2$H$_4$ and C$_2$H$_6$ is the highest, 110 °C. This is because the increased HR slows the CSC process to a certain extent. When varying the OxyC, C$_2$H$_4$ is detected first when the OxyC is 21% at 100 °C. Here, C$_2$H$_6$ is first detected at 90 °C. C$_2$H$_4$ is detected last when OxyC is 10% and the temperature is 120 °C. For the same temperature, the C$_2$H$_4$ and C$_2$H$_6$ concentrations corresponding to 10% OxyC are the smallest, which is similar to the change pattern seen in CH$_4$ concentrations.

C$_2$H$_4$ and C$_2$H$_6$ concentrations are produced gradually and increase slowly until Stage 3. The C$_2$H$_4$ and C$_2$H$_6$ concentration curves are relatively close for different AFRs. The C$_2$H$_4$ and C$_2$H$_6$ concentration curves intersect at 0.5 and 0.6 °C min^{-1}. Although the C$_2$H$_6$ concentration varies under different OxyCs, the C$_2$H$_4$ concentration curves under 3%, 7%, and 15% OxyCs are similar. The temperature at which the first gasses are detected is not the same, and so the effect of different conditions on C$_2$H$_4$ and C$_2$H$_6$ production before Stage 3 is unremarkable. The C$_2$H$_4$ and C$_2$H$_6$ concentrations at 40 and 80 mL min^{-1} AFRs differ above 150 °C, whereas at 120 and 160 mL min^{-1} AFRs, they differ above 140 °C. The C$_2$H$_4$ and C$_2$H$_6$ concentration curves at HRs 0.3, 0.4, 0.5, and 0.6 °C·min^{-1} are almost coincident. However, the C$_2$H$_4$ and C$_2$H$_6$ concentrations at HRs 0.3 and 0.4 °C min^{-1} differ noticeably above 170 °C. There is a noticeable difference between the C$_2$H$_4$ and C$_2$H$_6$ concentration curves under different OxyCs, and that difference increase with temperature. Therefore, OxyC has a substantial influence on C$_2$H$_4$
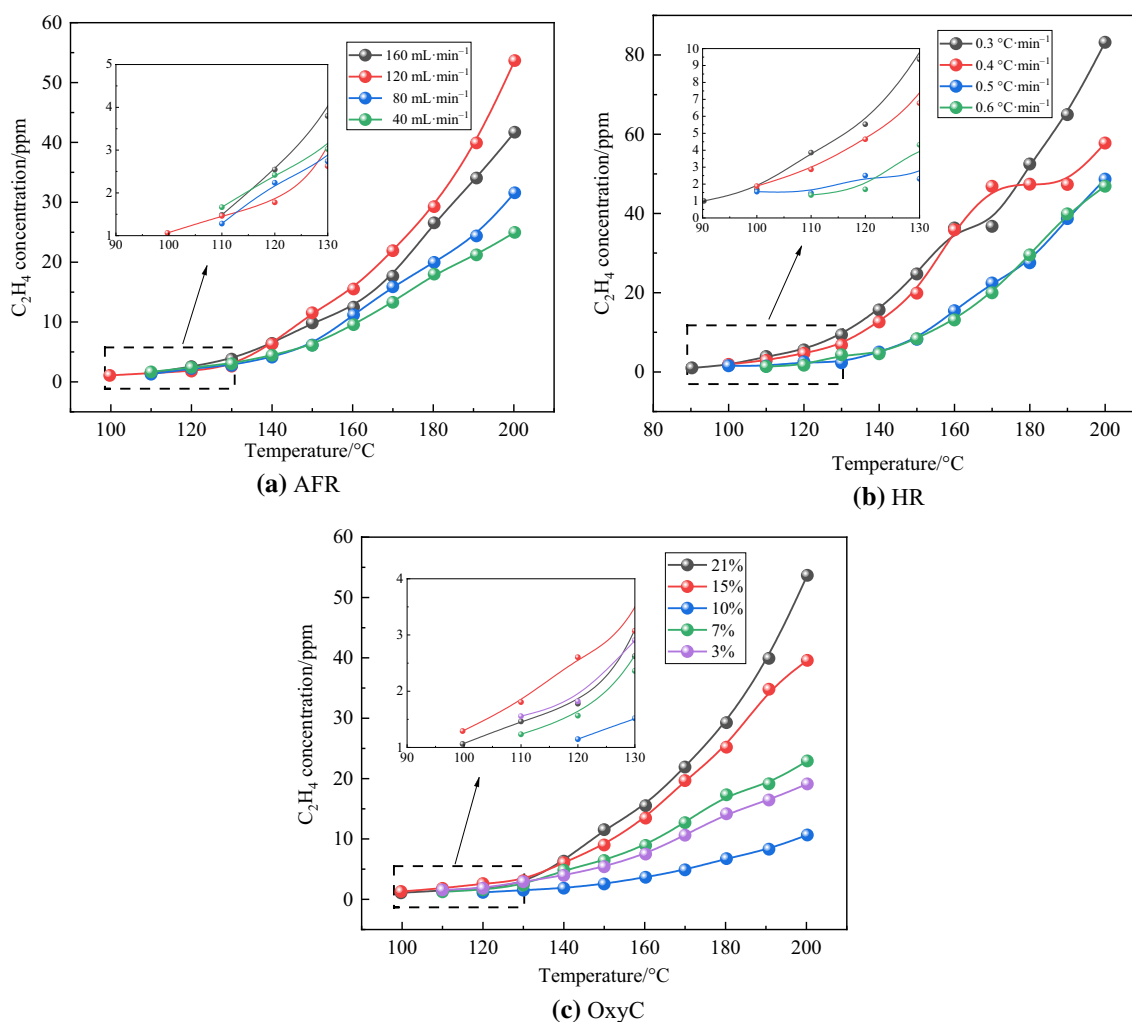
Fig. 11 C$_2$H$_4$ concentration curves at different temperatures, under multivariate conditions for **a** AFR, **b** HR, and **c** OxyC

and C$_2$H$_6$ generation in Stage 3. This suggests that the mass of OxyC in the coal oxygen reaction has a larger relative influence on the production of these two hydrocarbons.

Exothermic intensity

In Figs. 13 and 14, the exothermic intensity of the coal samples shows a positive correlation with the rise in temperature under different conditions. This is consistent with research by Wang et al. [54]. At lower temperatures, methylene is the initial active group and undergoes chemisorption to form hyperoxide. Heat at this stage is mainly chemisorption heat. As the coal temperature rises, the hyperoxide gradually decomposes and releases an immense amount of heat, and the free radicals produce accelerated the reaction, releasing even more heat. After reaching Stage 3, the heat release of the hydrocarbon gases begins to increase extraordinarily due to the fracturing of the active functional groups, such as the

aliphatic hydrocarbon side chains within the coal molecules [55, 56]. In addition, the oxidation products react with the active hydrogen in the benzene ring side chain to produce active reducing groups. The heat that this released supplies the active groups with enough thermal energy to begin free radical chain oxidation [57].

At the same temperature, exothermic intensity increases with the AFR, when it is below 120 mL min^{-1}. However, when the AFR exceeds 120 mL min^{-1}, the heat release starts to decline. This decrease is attributed to two factors: first, the coal oxygen reaction is partially inhibited; and second, the excessive air is transporting some of the heat generated away from the reaction. Furthermore, as the HR increases, the exothermic intensity gradually diminishes. The exothermic intensity at 0.3 °C min^{-1} HR is attenuated above 160 °C, and then increases rapidly. The exothermic intensity at HRs 0.4, 0.5, and 0.6 °C min^{-1} tends to be consistent above 160 °C, which corresponds to the changes observed in OxyC as
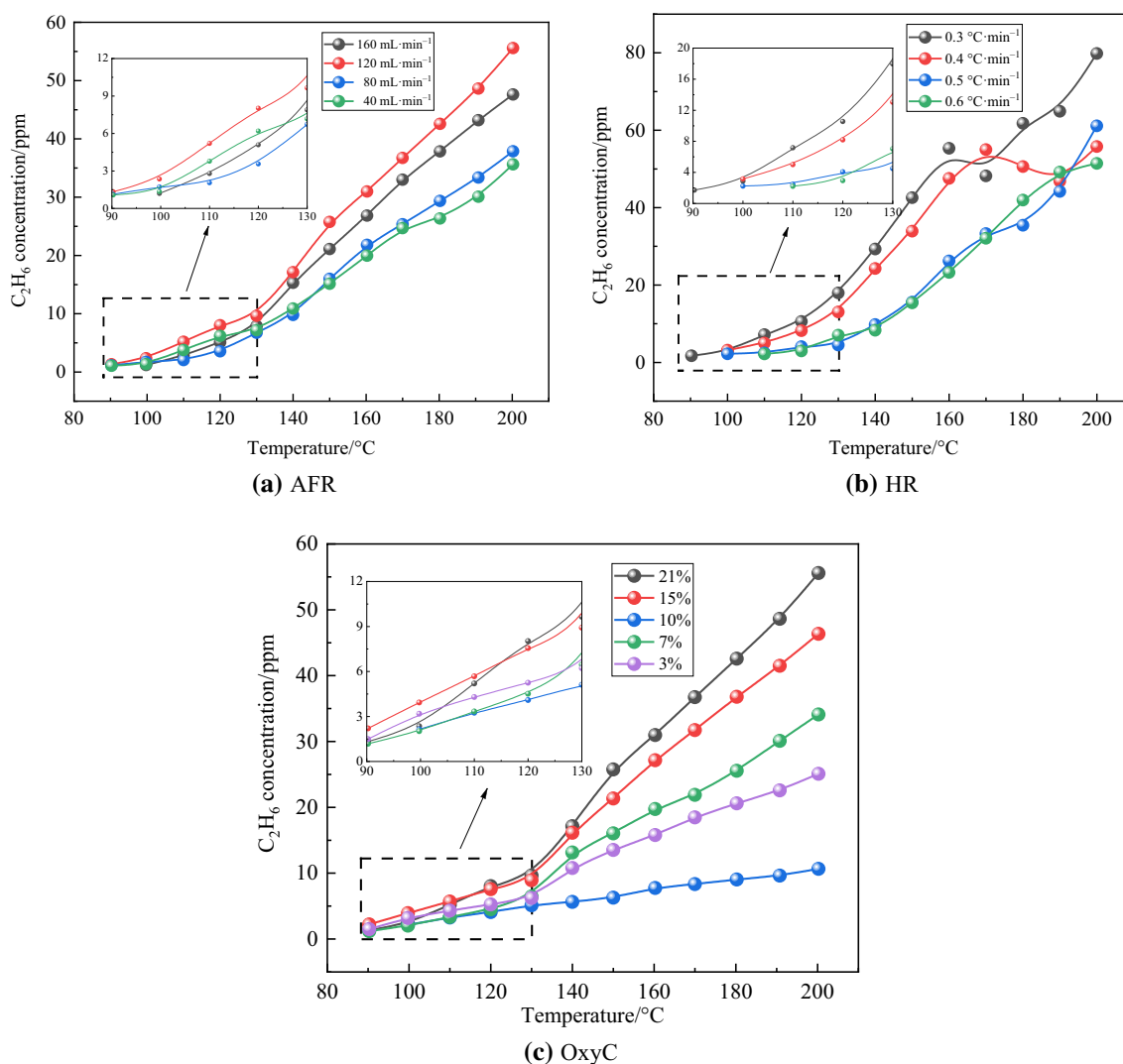
(a) AFR

(b) HR

(c) OxyC

Fig. 12 C_2H_6 concentration curves at different temperatures, under multivariate conditions for **a** AFR, **b** HR, and **c** OxyC

temperature changed. When OxyC varies, as temperature increases, the exothermic intensity is highest at 21%, and where OxyC is 10%, the exothermic intensity is low, only increasing slowly. A 10% OxyC inhibits the generation of active functional groups. This results in a reduction in the available active groups for oxygen reaction, and this results in a reduction in the amount of heat released as well.

In Stage 1, the exothermic intensity does not increase under AFR of 40, 80, or 160 mL min^{-1}. The heat release under an AFR of 120 mL min^{-1} is much larger than other AFRs. The exothermic intensity curves corresponding to different HRs and OxyCs are similar. At this stage, the chemisorption structures of the different active groups used to yield hyperoxide are basically the same [58], and so the levels of heat generated are also similar.

In Stage 2, the exothermic intensity under an AFR of 160 mL min^{-1}, and 40 as well as 80 mL min^{-1} AFR begins to differ after 100 °C. However, the exothermic intensity under AFRs of 40 and 80 mL min^{-1} remains similar. Although the exothermic intensities under different HRs start to be observable, the difference remains small. Except for the sudden change of heat release under a 21% OxyC, above 120 °C, the difference in heat release for other OxyCs remains small.

In Stage 3, the exothermic intensity under different AFRs and OxyCs is considerably different. Apart from the instant growth of the HR at 0.3 °C min^{-1}, the other differences are small. This means that changes in AFR and OxyC will have a large impact on heat storage.
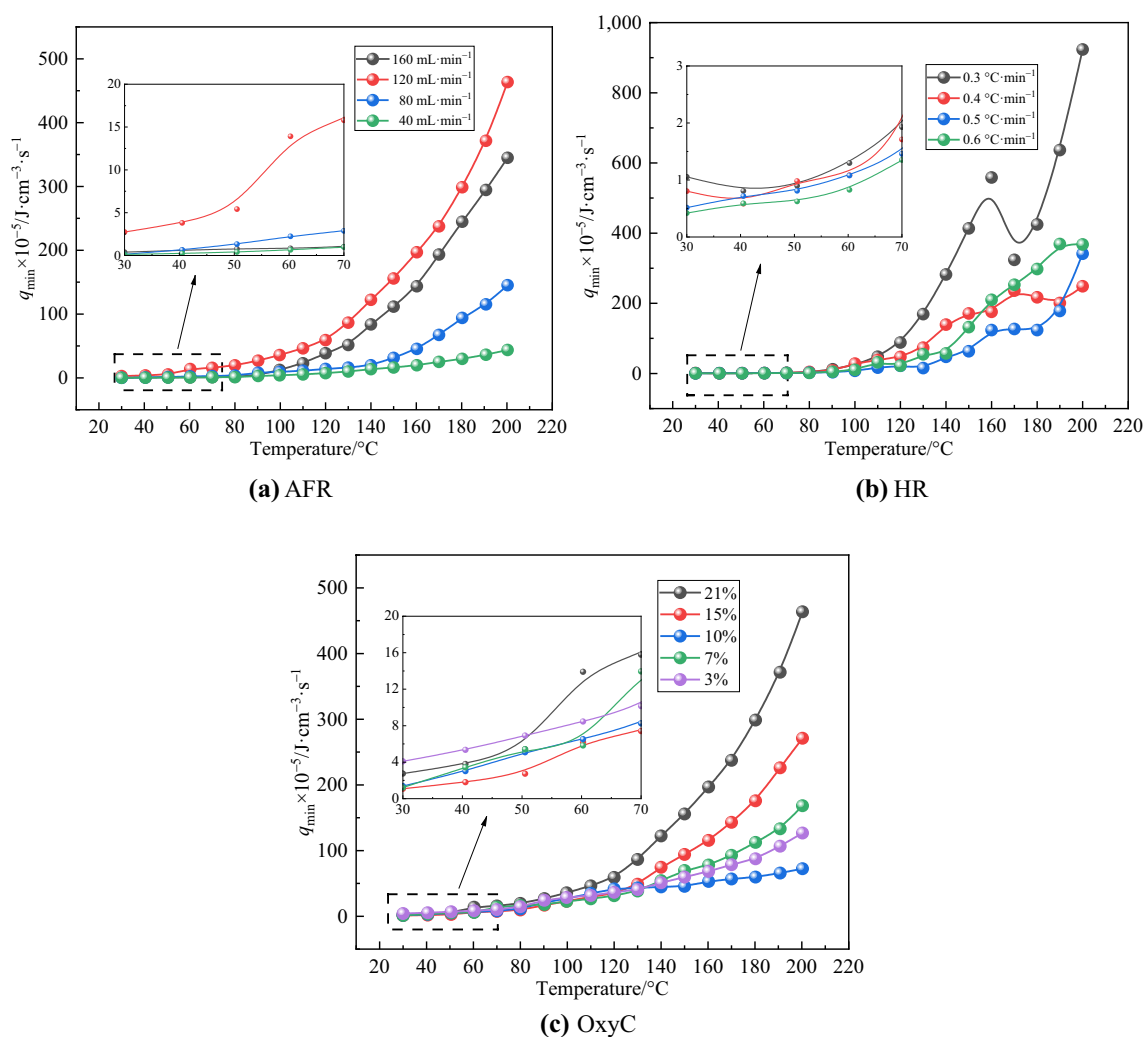
Fig. 13 q_{min} curves at different temperatures under multivariate conditions for **a** AFR, **b** HR, and **c** OxyC

Analysis of apparent activation energy

Following Eq. (5), the linear relationships between $ln[v\ O_2/C1\ O_2]$ and $1/T$ under different conditions were computed.

Effect of airflow on apparent activation energy

Figure 15 shows the linear fitting equation, and E_a for different AFRs, and the data are tabulated in Table 3. It can be seen from Table 3 that the R^2 is greater than 0.96, so it is a particularly strong relationship. The E_a required for coal oxidation initially decreases, then increases as AFR increases. For an AFR of 120 mL min^{-1}, the energy needed for the coal molecules to shift from their normal state to an active state (i.e., predisposed to chemical reaction), is at its lowest. This signifies the highest propensity for CSC. When the AFR exceeds 120 mL min^{-1}, the E_a required begins to increase.

An AFR of 120 mL min^{-1} could be considered the critical AFR for the chemical reaction in this sample. When the AFR reaches 160 mL min^{-1}, the E_a is the highest, making CSC relatively difficult. This is mainly a result of the AFR transporting heat away from the reaction and an increase in heat dissipation around the sample.

Effect of heating rate on apparent activation energy

Figure 16 shows the linear fitting of E_a for different HRs, and the same data are tabulated in Table 4. As shown in Table 4, the E_a of the coal samples decreases as HR increases. When the HR is 0.3 °C min^{-1}, the required E_a is the largest, at ca. 46.92 kJ mol^{-1}; when the HR increases from 0.3 to 0.4 °C min^{-1}, the E_a decreases substantially. When the HR increases to 0.6 °C min^{-1}, the E_a remains relatively stable at roughly 40 kJ mol^{-1}. This is because, with different HRs, the coal body reaches the
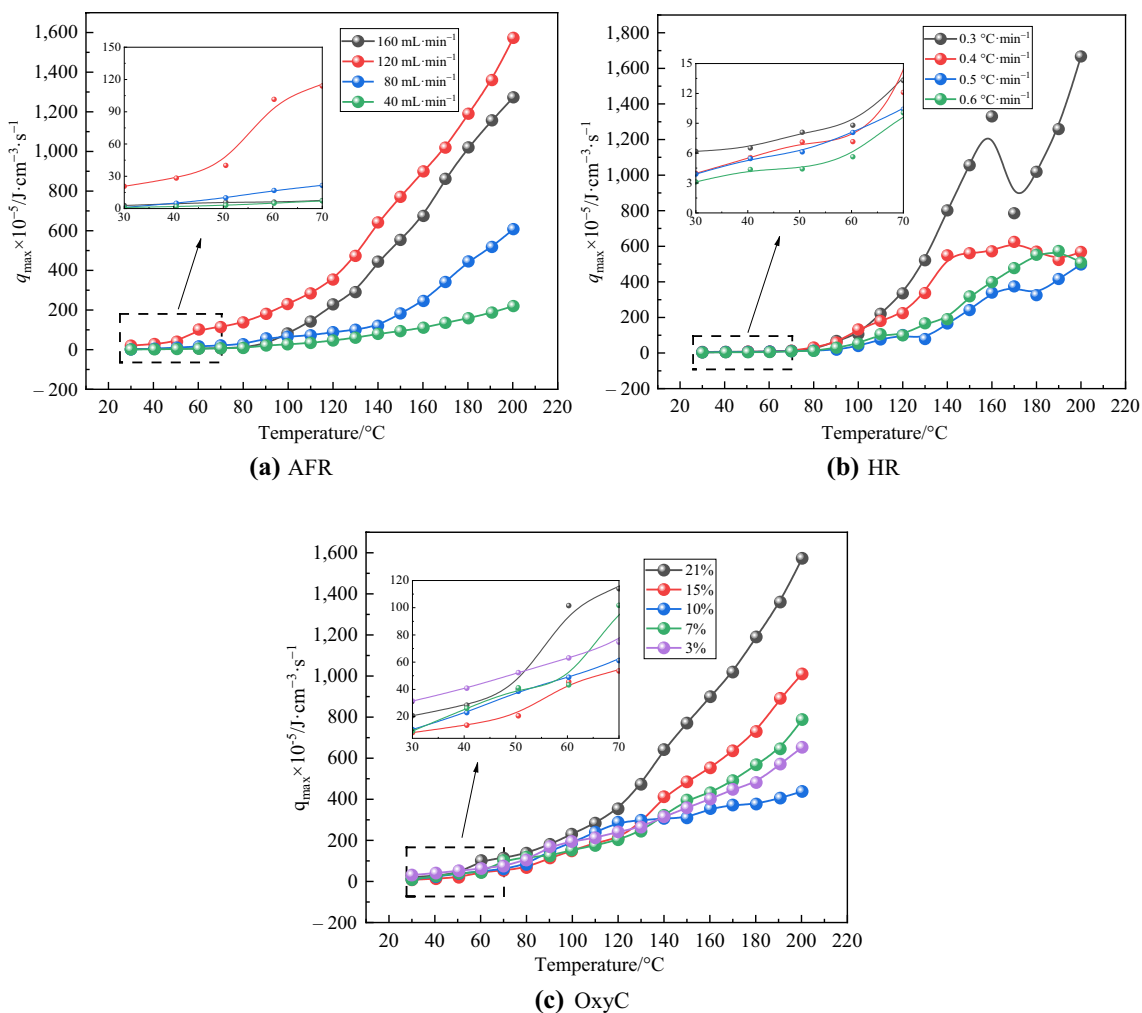
(a) AFR

(b) HR

(c) OxyC

Fig. 14 q_{max} curves at different temperatures, under multivariate conditions for **a** AFR, **b** HR, and **c** OxyC

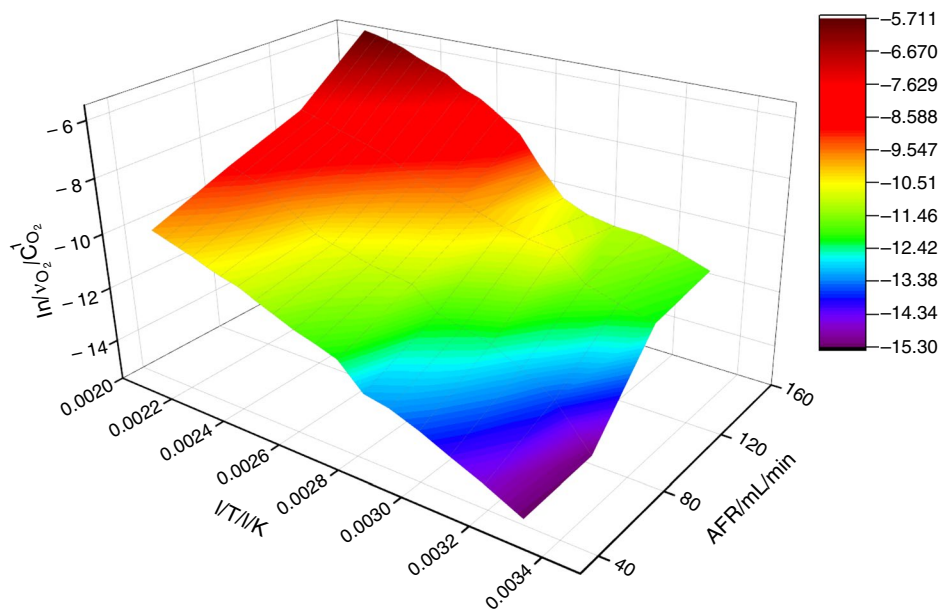**Fig. 15** $ln[v\,O_2/C1\,O_2]$ and $1/T$ plots under different AFR

Table 3 E_a of coal samples calculated using Arrhenius equation under different AFRs

AFR/mL min^{-1}	Linear relation	R^2	E_a/Kj mol^{-1}
40	$y = -4586.9x + 0.1$	0.9896	38.14
80	$y = -4648.8x + 1.1$	0.9648	38.65
120	$y = -3744.6x + 0.2$	0.9897	31.13
160	$y = -6034.4x + 7.4$	0.9602	50.17

Table 4 E_a of coal samples calculated using Arrhenius equation under different HRs

HR/°C min^{-1}	Linear relation	R^2	E_a/kJ mol^{-1}
0.3	$y = -5643.5x + 6.8$	0.9348	46.92
0.4	$y = -5044.6x + 4.9$	0.9247	41.94
0.5	$y = -4603.8x + 3.1$	0.9679	38.28
0.6	$y = -4939.3x + 4.1$	0.8877	41.07

same temperature in a shorter time, resulting in a faster overall reaction. The smaller the HR, the longer the time required to reach the same temperature. This leads to a more thorough coal oxidation reaction, and where some active groups have lower E_a, they are able to react first, releasing heat. As the temperature increases, more groups with different types and quantities of active components participate in the reaction, resulting in a higher E_a. When the HR is greater than 0.4 °C min^{-1}, the coal oxygen reaction does not reach the energy required for some active functional groups to participate, thereby leading to a lower E_a, as reflected in the OxyC change diagram.

Effect of oxygen concentration on apparent activation energy

Figure 17 shows the linear equation and E_a for different OxyC. The same data are presented in Table 5, where the E_a shows a law of fluctuating growth with OxyC. When the OxyC is 3%, the E_a of the coal sample is the smallest, at approximately 21.77 kJ mol^{-1}. As OxyC increases, E_a also gradually increases. When the OxyC is 15%, the E_a is the

largest, at 34.01 kJ mol^{-1}. The main reason for this might be that the more stable macromolecular structures in the sample gradually decompose into multiple small molecular structures as reaction temperature increases, resulting in more active sites. A decrease in OxyC led to fewer oxygen molecules being available for participation in the reaction, leading to a lower number of active groups being available to react with the oxygen. As a result, the energy required for the reaction decreased, and E_a decreased accordingly.

Comparison of apparent activation energy levels under different conditions

Figure 18 shows the E_a of coal samples under different conditions. The E_a under different OxyC conditions range between 20 and 35 kJ mol^{-1}, whereas the E_a under different AFR and HR conditions is between 30 and 50 kJ mol^{-1}. E_a is the greatest when the HR does not exceed 0.5 °C min^{-1}. When AFR exceeds 120 mL min^{-1}, E_a increased sharply and gradually surpasses the corresponding E_a under the HR condition to reach its maximum. Except for the E_a at 15% OxyC, because this is greater than the corresponding
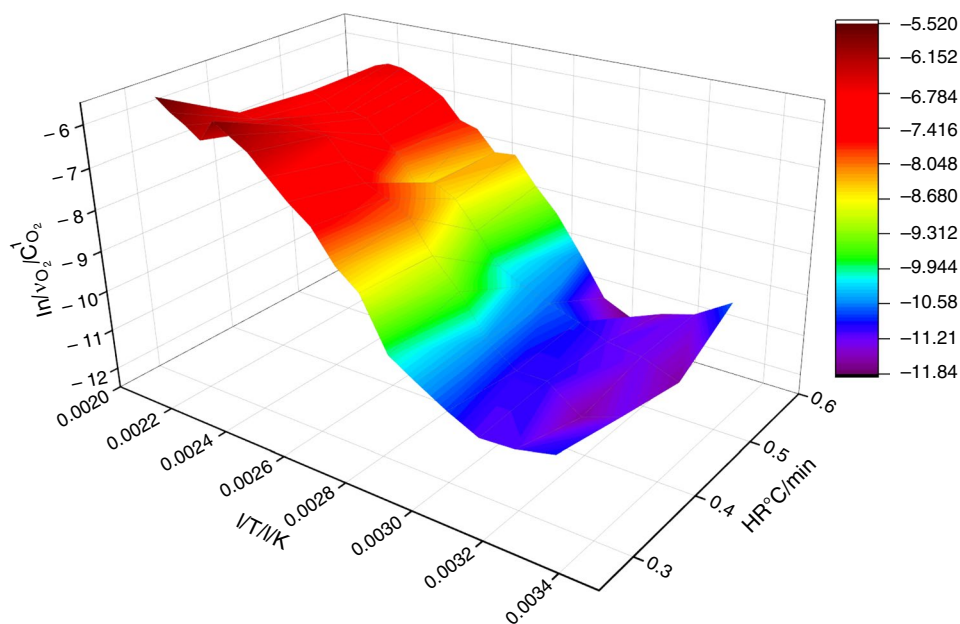
Fig. 16 $ln[vO2/C1\ O_2]$ and $1/T$ plots under different HR

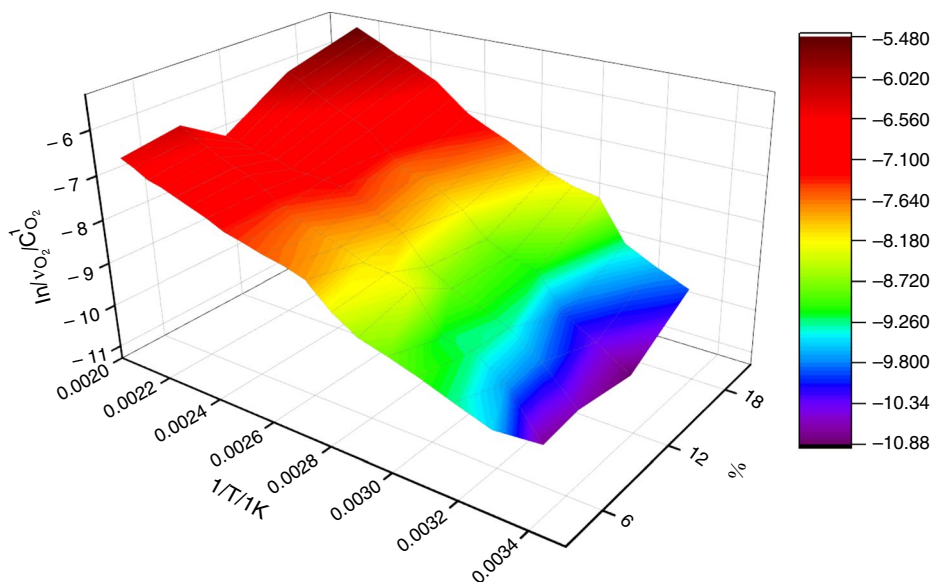**Fig. 17** $\ln[v\,O_2/C1\,O_2]$ and $1/T$ plots under different OxyC

Table 5 E_α of coal samples calculated using Arrhenius equation under different OxyCs

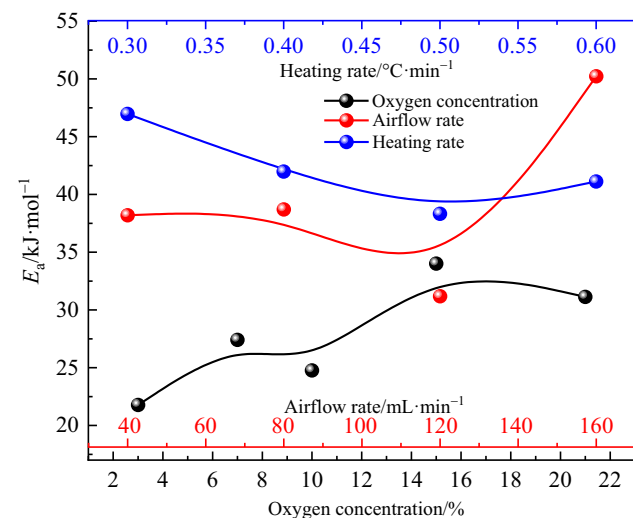| OxyC/% (%)	Linear relation	R^2	E_a/kJ mol^{-1}
3	$y = -2618.8x - 0.9$	0.9877	21.77
7	$y = -3297.2x + 0.8$	0.9635	27.41
10	$y = -2977.6x - 0.1$	0.9216	24.76
15	$y = -4090.4x + 2.9$	0.9902	34.01
21	$y = -3744.7x + 2.5$	0.9897	31.13

Fig. 18 Change in E_a under multivariate conditions

E_a at 120 mL min^{-1} AFR, E_a is always the smallest under the OxyC condition, indicating that coal is more prone to reactions. The variation range of E_a of the samples under different AFRs is the largest, thus yielding the greatest effect on CSC tendency.

Analysis of the changes to characteristic parameters with experimental conditions

Based upon the experimental data, there are numerous instances where multiple experimental conditions were pronouncedly impacting a specific parameter, within the same stage. For instance, it was observed that in Stage 3, AFR and OxyC exerted a considerable influence on exothermic intensity. To accurately assess the influence of experimental conditions on characteristic parameters, the one-way analysis of variance (ANOVA) was applied. This method alters one experimental condition at a time, thereby isolating its effect on the characteristic parameters from other factors. AFR, OxyC, and HR conditions are treated as independent variables, while the characteristic parameter values are treated as dependent variables, allowing for a quantitative analysis of the influence of different conditions on CSC characteristic parameters across various stages.

Taking the effect of AFR on CO concentration, as an example, the specific steps of one-way ANOVA calculation are as follows:

1. Group the CO concentration data based on the experimental conditions into i groups, each containing j CO concentration data points.
2. Calculate the sum of squares total (SST), the sum of squares between (SSB), and the sum of squares within (SSW):

$$SS_T = \sum_{i=1,j=1}^{m,n} \left(x_{ij} - \bar{\bar{x}} \right)^2 \qquad (7)$$

$$SS_B = \sum_{i=1}^{m} \left(\bar{x}_i - \bar{\bar{x}} \right)^2 \qquad (8)$$

$$SS_W = \sum_{i=1}^{m} \sum_{j=1}^{n} \left(x_{ij} - \bar{x}_i \right)^2 \qquad (9)$$

3. Divide the sum of squares by the corresponding degrees of freedom to reduce the effect of sample size on the sum of squares, obtaining the mean square between (MSB) and the mean square within (MSW):

$$MS_B = \frac{SS_B}{m-1} \qquad (10)$$

$$MS_W = \frac{SS_W}{N-m} \qquad (11)$$

4. Use the F-distribution to test the significant impact of the independent variable on the dependent variable:

$$F = \frac{MS_B}{MS_W} \qquad (12)$$

5. Calculate the effect size of the independent variable on the dependent variable using the partial η^2 value:

$$\eta^2 = \frac{SS_B}{SS_T} \qquad (13)$$

Using these formulae, the impact of changes in AFR on CO concentration at different stages of CSC can be reckoned, and the results are presented in Tables 6, 7, and 8.

Through Tables 6–8, it can be observed that in Stage 1, F = 3.16864 < F crit = 3.23887, in Stage 2, F = 4.09207 > F crit = 3.23887, and in Stage 3, F = 8.02601 > F crit = 2.94669. This indicates that in Stage 1, changes in AFR have a less significant effect on CO concentration. In contrast, in Stages 2 and 3, the influence of AFR on CO concentration is more prominent. Further analysis revealed that the partial η^2 under Stage 3 is greater than the partial η^2 in Stage 2, indicating that AFR has a greater impact on CO concentration in Stage 3 than in Stage 2. Based upon this analysis, it can be concluded that as temperature rises during CSC, the influence of AFR on CO concentration changes notably.

Similarly, employing the aforementioned method to analyse the CSC characteristic parameters under different

Table 6 Variance analysis results of the impact of AFR changes on CO concentration in Stage 1

Source of variance	SS	Df	MS	F	F crit	Partial η^2
Between-class	8646.88	3	2882.29	3.12	3.24	0.37
Intra-class	14,554.10	16	909.63			
Total	23,200.98	19				

SS sum of square; *Df* degree of freedom; *MS* mean square; *F* F-statistic; *F crit* F critical value; and Partial η^2 effect size

Table 7 Variance analysis results of the impact of AFR changes on CO concentration in Stage 2

Source of variance	SS	Df	MS	F	F crit	Partial η^2
Between-class	1,601,767.76	3	533,922.59	4.09	3.24	0.43
Intra-class	2,087,640.47	16	130,477.53			
Total	3,689,408.23	19				

SS sum of square; *Df* degree of freedom; *MS* mean square; *F* F-statistic; *F crit* F critical value; and partial η^2 effect size

Table 8 Variance analysis results of the impact of AFR changes on CO concentration in Stage 3

Source of variance	SS	Df	MS	F	F crit	Partial η^2
Between-class	185,329,721.89	3	61,776,573.96	8.03	2.95	0.46
Intra-class	215,517,367.87	28	7,697,048.85			
Total	400,847,089.76	31				

SS sum of square; *Df* degree of freedom; *MS* mean square; *F* F-statistic; *F crit* F critical value; and partial η^2 effect size
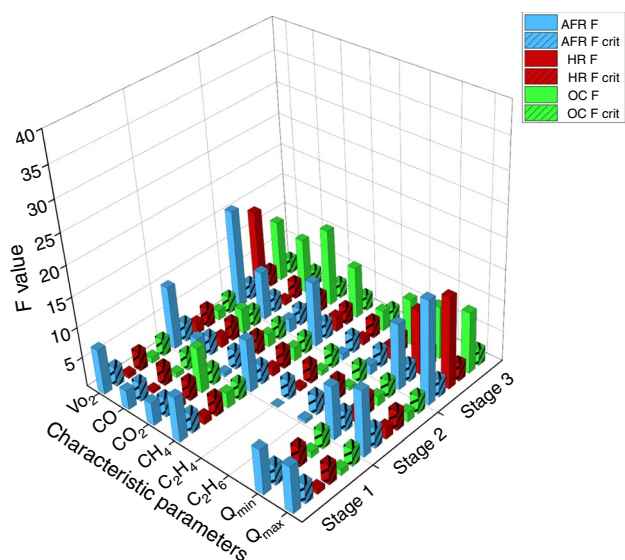
Fig. 19 Change of F value of the characteristic parameters under multivariate conditions
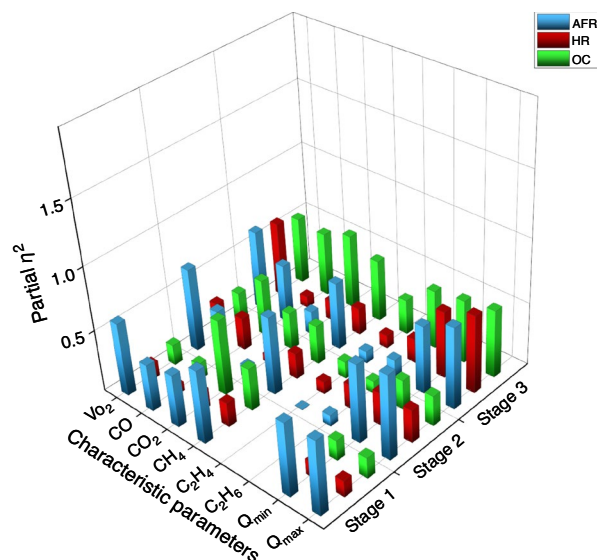

Fig. 20 Change of partial eta square value of the characteristic parameters under multivariate conditions

conditions yields the results shown in Figs. 19 and 20. That is, through a longitudinal comparison of partial η^2 values and considering the magnitudes of the F values and F crit values, changes in AFR differentially affect oxygen consumption rate, CH_4, Q_{min}, and Q_{max} at different stages of CSC, with the most pronounced impact being observed in Stage 2. It also has a significant effect on CO_2 concentration in Stage 1 and CO concentration after Stage 1, with a greater impact on CO concentration in Stage 3 compared with Stage 2. There is no significant impact on C_2H_4 and C_2H_6 concentrations, but the overall impact on C_2H_4 and C_2H_6 concentrations shows an increasing trend.

Changes in HR only show a significant impact on the oxygen consumption rate, Q_{min}, and Q_{max} in Stage 3, with no notable impact on parameters in other conditions. However, by comparing the partial η^2, it can be seen that as the coal oxidation degree increases, the influence of HR change on CO concentration first increases, then decreases. However, the influence on CO_2 concentration is the opposite (first decreasing, then increasing). The effects on hydrocarbon gases are similar at all stages.

Changes in OxyC had a significant impact on all parameters in Stage 3, and additionally, had a significant impact on CO in Stage 2, and CO_2 concentration in Stage 1. It shows that the effect of OxyC on the spontaneous combustion process of coal is mainly reflected in Stage 3. However, it is worth noting that in Stage 3, the influence of OxyC on oxygen consumption rate, CH_4 and exothermic intensity is less than that of AFR. The impact on CO concentration in Stage 3 is greater than it was in Stage 2; yet the impact on CO_2 concentration in the Stage 1 is greater than it was in Stage 3, with no distinct impact being observed in other conditions.

In general, as reaction temperature increases, the influence of OxyC on CO_2 and CH_4 concentration first decreases, then increases, while the other parameters show an overall increasing trend. To further assess which factor demonstrated the greatest impact when changes in condition noticeably affected the same parameter in the same stage, a horizontal comparison of partial eta values was used. In this case, changes in OxyC have the greatest impact on CO concentration in Stage 2, and on CO_2 concentration in Stages 1 and 3. The impact of changes in AFR on the oxygen consumption rate, CH_4, Q_{min}, and Q_{max} in Stage 3 is greater than the impact of changes in OxyC and HR.

Thus, changes in AFR exhibit the greatest impact on oxygen consumption rate, CH_4, Q_{min}, and Q_{max} at all stages. Changes in OxyC have the greatest impact on CO, CO_2, C_2H_4, and C_2H_6 in Stage 3, and they also have the greatest impact on CO_2 in Stage 1, and on CO concentration in Stage

Table 9 Factors that exert greatest influence on CSC characteristic parameters at different stages

	Stage		
	Stage 1	Stage 2	Stage 3
VO_2	AFR	AFR	AFR
CO	–	OxyC	OxyC
CO_2	OxyC	–	OxyC
CH_4	AFR	AFR	AFR
C_2H_4 C_2H_6	–	–	OxyC
Exothermicity	AFR	AFR	AFR

– not applicable

2. In all other cases, changes in the various conditions have no conspicuous impact on characteristic parameters, as listed in Table 9.

Conclusions

In this study, programmed temperature experiments were conducted to investigate the changes in characteristic parameters of coal samples under different conditions, analyse the E_a of the coal-oxygen reaction, and quantitatively evaluate the impact of experimental conditions on CSC parameters. The main conclusions were:

- The critical temperature of coal samples ranged from 65 to 75 °C, and the cracking temperature ranges from 115 to 130 °C. The low-temperature oxidation process of coal can be divided into three stages, with similar trends in characteristic parameter changes at each stage. The E_a under OxyC conditions was generally lower than under AFR and HR conditions.
- AFR changes prominently impact oxygen consumption rate, CH_4, and exothermic intensity, especially in Stage 2, with partial η^2 values greater than 0.6. HR did not significantly affect carbon–oxygen gases. The impact of OxyC on CO_2 and CH_4 initially decreased and then increased (partial η^2 trend was $0.6 \rightarrow 0.3 \rightarrow 0.59$ and $0.34 \rightarrow 0.31 \rightarrow 0.49$, respectively). In other cases, the impact of external condition changes on characteristic parameters increased with temperature.
- Above the cracking temperature, changes in OxyC had the greatest impact on CO, CO_2, C_2H_4, and C_2H_6, with partial η^2 values of 0.51, 0.59, 0.278, and 0.45, respectively. In addition, OxyC had the most significant impact on CO_2 in Stage 1 and CO concentration in Stage 2. In other scenarios, changes in conditions did not substantially affect CSC characteristic parameters.

Declarations

References

1. Gao ZG. Sustainable development and upgrading mode of coal industry in China. Int J Min Sci Technol. 2012;22(3):335–40.
2. Pan RK, Cheng YP, Yu MG, Lu C, Yang K. New technological partition for "three zones" spontaneous coal combustion in goaf. Int J Min Sci Technol. 2013;23(4):489–93.
3. Singh N, Chatterjee RS, Kumar D, Panigrahi DC. Spatio-temporal variation and propagation direction of coal fire in Jharia Coalfield, India by satellite-based multi-temporal night-time land surface temperature imaging. Int J Min Sci Technol. 2021;31(5):765–78.
4. Shao SH, Wu CL, Hao M, Song XL, Su XY, Wang WH, Li GS, Shi BB. A novel coating technology for fast sealing of air leakage in underground coal mines. Int J Min Sci Technol. 2021;31(2):313–20.
5. Xia TQ, Zhou FB, Wang XX, Zhang YF, Li YM, Kang JH, Liu JS. Controlling factors of symbiotic disaster between coal gas and spontaneous combustion in longwall mining gobs. Fuel. 2016;182:886–96.
6. Yuan LM, Smith AC. The effect of ventilation on spontaneous heating of coal. J Loss Prev Process Ind. 2012;25(1):131–7.
7. Yang SQ, Zhou BZ, Wang CJ. Investigation on coal spontaneous combustion in the gob of Y type ventilation caving face: a case study. Process Saf Environ Prot. 2021;148:590–603.
8. Zhao JY, Lu SP, Song JJ, Zhang YX, Zeng Q, Shu CM. Evaluation of oxygen concentration on low-temperature oxidation kinetics of long-flame coal. J Loss Prev Process Ind. 2022;79:104841.
9. Zhao JY, Zhang YL, Song JJ, Guo T, Deng J, Shu CM. Oxygen distribution and gaseous products change of coal fire based upon the semi-enclosed experimental system. Energy. 2023;263:125721.
10. Zhang YT, Zhang YB, Li YQ, Shi XQ, Zhang YJ. Heat effects and kinetics of coal spontaneous combustion at various oxygen contents. Energy. 2021;234:121299.
11. Zhou BZ, Yang SQ, Wang CJ, Hu XC, Song WX, Cai JW, Xu Q, Sang NW. The characterization of free radical reaction in coal low-temperature oxidation with different oxygen concentration. Fuel. 2020;262:116524.
12. Lü HF, Deng J, Li DJ, Xu F, Xiao Y, Shu CM. Effect of oxidation temperature and oxygen concentration on macro characteristics of pre-oxidised coal spontaneous combustion process. Energy. 2021;227:120431.
13. Ren LF, Deng J, Li QW, Ma L, Zou L, Wang BL, Shu CM. Low-temperature exothermic oxidation characteristics and spontaneous combustion risk of pulverised coal. Fuel. 2019;252:238–45.
14. Xiao Y, Guo T, Shu CM, Li QW, Li DJ, Chen LG. Effects of oxygen concentrations on the coal oxidation characteristics and functional groups. J Therm Anal Calorim. 2020;142(2):899–912.
15. Zhong XX, Li LD, Chen Y, Dou GL, Xin HH. Changes in thermal kinetics characteristics during low-temperature oxidation of low-rank coals under lean-oxygen conditions. Energy Fuels. 2017;31(1):239–48.
16. Perdochova M, Derychova K, Veznikova H, Bernatik A, Pitt M. The influence of oxygen concentration on the composition of gaseous products occurring during the self-heating of coal and wood sawdust. Process Saf Environ Prot. 2015;94:463–70.
17. Shen J, Zhu HQ, Zhang Z. Experiment analysis of relationship between oxygen concentration and coal oxidation characteristics. Metall Min Ind. 2015;6:617–22.

18. Wang G, Xie J, Xue S, Wang HY. Laboratory study on low-temperature coal spontaneous combustion in the air of reduced oxygen and low methane concentration. Teh Vjesn. 2015;22(5):1319–25.

19. Wen H, Guo J, Jin YF, Wang K, Zhang Y, Zheng X. Experimental study on the influence of different oxygen concentrations on coal spontaneous combustion characteristic parameters. Int J Oil Gas Coal Technol. 2017;16(2):187–202.

20. Song JJ, Deng J, Zhao JY, Zhang YN, Shu CM. Comparative analysis of exothermic behaviour of fresh and weathered coal during low-temperature oxidation. Fuel. 2021;289:119942.

21. Liu X, Tan HZ, Wang XB, Wang Z, Xiong XH. Oxidation reactivity and kinetic analysis of bituminous coal char from high-temperature pyrolysis: effect of heating rate and pyrolysis temperature. Thermochim Acta. 2020;690:178660.

22. Zhai XW, Ge H, Shu CM, Obracaj D, Wang K, Wang BL. Effect of the heating rate on the spontaneous combustion characteristics and exothermic phenomena of weakly caking coal at the low-temperature oxidation stage. Fuel. 2020;268:117327.

23. Yang XY, Wei R, Qin WG, Hu CJ, Xiao Y, Zhao JR, Tian SL, Zang K, Wang D, Tian LY. Thermal effects and kinetics behaviors of coal spontaneous combustion via synchronous thermal analyzer under different heating rates. Combust Sci Technol. 2022;196:1–14.

24. Zhang Y, Li YQ, Huang Y, Li SS, Wang WF. Characteristics of mass, heat and gaseous products during coal spontaneous combustion using TG/DSC–FTIR technology: the impacts of oxygen concentrations and heating rates. J Therm Anal Calorim. 2018;131:2963–74.

25. Li QW, Xiao Y, Wang CP, Deng J, Shu CM. Thermokinetic characteristics of coal spontaneous combustion based on thermogravimetric analysis. Fuel. 2019;250:235–44.

26. Onifade M, Genc B, Bada S. Spontaneous combustion liability between coal seams: a thermogravimetric study. Int J Min Sci Technol. 2020;30(5):691–8.

27. Guo J, Yan H, Liu Y, Li SS. Preventing spontaneous combustion of coal from damaging ecological environment based on thermogravimetric analysis. Appl Ecol Environ Res. 2019;17(4):9051–64.

28. Deng J, Zhang YX, Zhao JY, Song JJ, Zhang YN. Experiment study on oxidation and activated energy of different particle size coal based on programmed temperature rising. Coal Sci Technol. 2019;47(1):214–9.

29. Ma L, Zou L, Ren LF, Chung YH, Zhang PY, Shu CM. Prediction indices and limiting parameters of coal spontaneous combustion in the Huainan mining area in China. Fuel. 2020;264:116883.

30. Wen H, Xu JC, Ge LM, Deng J. Technique of measurement and test of coal spontaneous combustion characteristic and numerical analysis. J Univ Sci Technol. 2001;23(6):499–501 ((**In Chinese**)).

31. Xu JC. Determination theory of coal spontaneous combustion zone. Beijing, China: China Coal Ind Publ House; 2001. ((**In Chinese**)).

32. Song JJ, Deng J, Zhao JY, Zhang YN, Wang CP, Shu CM. Critical particle size analysis of gas emission under high-temperature oxidation of weathered coal. Energy. 2021;214:118995.

33. Ren LF, Li QW, Deng J, Ma L, Xiao Y, Zhai XW, Hao JC. Effect of oxygen concentration on the oxidative thermodynamics and spontaneous combustion of pulverized coal. ACS Omega. 2021;6(40):26170–9.

34. Yan H, Nie B, Liu P, et al. Experimental investigation and evaluation of influence of oxygen concentration on characteristic parameters of coal spontaneous combustion. Thermochim Acta. 2022;717:179345.

35. Deng J, Zhao JY, Zhang YN, Geng RL. Study on coal spontaneous combustion characteristic temperature of growth rate analysis. Proc Eng. 2014;84:796–805.

36. Xu Q, Yang SQ, Tang ZQ, Cai JW, Zhong Y, Zhou BZ. Free radical and functional group reaction and index gas CO emission during coal spontaneous combustion. Combust Sci Technol. 2018;190(5):834–48.

37. Onifade M, Genc B. A review of research on spontaneous combustion of coal. Int J Min Sci Technol. 2020;30(3):303–11.

38. Itay M, Hill CR, Glasser D. A study of the low temperature oxidation of coal. Fuel Process Technol. 1989;21(2):81–97.

39. Zhao JY, Hang G, Song JJ, Lu SP, Ming HQ, Chang JM, Deng J, Zhang YN, Shu CM. Spontaneous oxidation kinetics of weathered coal based upon thermogravimetric characteristics. Energy. 2023;275:127489.

40. Zhao JY, Deng J, Song JJ, Shu CM. Effectiveness of a high-temperature-programmed experimental system in simulating particle size effects on hazardous gas emissions in bituminous coal. Safety Sci. 2019;115:353–61.

41. Qin BT, Lu Y, Jia YW. CO emission in the air return corner of the working face in shallow burial mining areas. Int J Min Sci Technol. 2014;24(5):617–23.

42. Deng J, Song JJ, Zhao JY, Zhang YN, Zhang YX, Shu CM. Gases and thermal behavior during high-temperature oxidation of weathered coal. J Therm Anal Calorim. 2019;138:1573–82.

43. Cai JW, Yang SQ, Hu XC, Song WX, Xu Q, Zhou BZ, Song YW. Forecast of coal spontaneous combustion based on the variations of functional groups and microcrystalline structure during low-temperature oxidation. Fuel. 2019;253:339–48.

44. Mohalik NK, Mandal S, Ray SK, Khan AM, Mishra D, Pandey JK. TGA/DSC study to characterise and classify coal seams conforming to susceptibility towards spontaneous combustion. Int J Min Sci Technol. 2022;32(1):75–88.

45. Deng J, Zhao JY, Zhang YN, Huang AC, Liu XR, Zhai XW, Wang CP. Thermal analysis of spontaneous combustion behavior of partially oxidized coal. Process Saf Environ Prot. 2016;104:218–24.

46. Zhao JY, Zhang YL, Song JJ, Zhang TH, Ming HQ, Lu SP, Deng J, Shu CM. Microstructure of coal spontaneous combustion in low-oxygen atmospheres at characteristic temperatures. Fuel. 2022;309:122132.

47. Zhao JY, Wang T, Deng J, Shu CM, Zeng Q, Guo T, Zhang YX. Microcharacteristic analysis of CH_4 emissions under different conditions during coal spontaneous combustion with high-temperature oxidation and in situ FTIR. Energy. 2020;209:118494.

48. Niu HY, Sun QQ, Bu YC, Chen HY, Yang YX, Li SP, Sun SW, Mao ZH, Tao M. Study of the microstructure and oxidation characteristics of residual coal in deep mines. J Clean Prod. 2022;373:133923.

49. Zhang L, Qi SC, Takeda N, Kudo S, Hayashi J, Norinaga K. Characteristics of gas evolution profiles during coal pyrolysis and its relation with the variation of functional groups. Int J Coal Sci Technol. 2018;5:452–63.

50. Zeng Q, Shen L. Experimental study on the oxidation kinetics of coal in typical coal mining areas of the Southern Junggar coalfield, Xinjiang, China. Int J Coal Sci Technol. 2022;9(1):78.

51. Jia HL, Yang Y, Ren WX, Kang ZH, Shi JT. Experimental study on the characteristics of the spontaneous combustion of coal at high ground temperatures. Combust Sci Technol. 2022;194(14):2880–93.

52. Zhao JY, Ming HQ, Song JJ, Lu SP, Xiao YY, Zhang YL, Shu CM. Preoptimal analysis of phase characteristic indicators in the entire process of coal spontaneous combustion. J Loss Prev Process Ind. 2023;84:105131.

53. Zhou CS, Zhang YL, Wang JF, Xue S, Wu JM, Chang LP. Study on the relationship between microscopic functional group and coal mass changes during low-temperature oxidation of coal. Int J Coal Geol. 2017;171:212–22.

54. Wang CP, Zhao XY, Bai ZJ, Deng J, Shu CM, Zhang M. Comprehensive index evaluation of the spontaneous combustion capability of different ranks of coal. Fuel. 2021;291:120087.

55. Wang DM, Xin HH, Qi XY, Dou GL, Qi GS, Ma LY. Reaction pathway of coal oxidation at low temperatures: a model of cyclic chain reactions and kinetic characteristics. Combust Flame. 2016;163:447–60.

56. Wang DM, Zhong XX, Gu JJ, Qi XY. Changes in active functional groups during low-temperature oxidation of coal. Min Sci Technol (China). 2010;20(1):35–40.

57. Zhao JY, Deng J, Chen L, Wang T, Song JJ, Zhang YN, Shu CM, Zeng Q. Correlation analysis of the functional groups and exothermic characteristics of bituminous coal molecules during high-temperature oxidation. Energy. 2019;181:136–47.

58. Clemens AH, Matheson TW, Rogers DE. Low temperature oxidation studies of dried New Zealand coals. Fuel. 1991;70(2):215–21.